# Downregulation of Semaphorin 4A in keratinocytes reflects the features of non-lesional psoriasis

**Authors:** Miki Kume [1], Hanako Koguchi-Yoshioka [1,2], Shuichi Nakai [1,3], Yutaka Matsumura [1], Atsushi Tanemura [1], Kazunori Yokoi [1], Shoichi Matsuda [1,3], Yuumi Nakamura [1.4], Naoya Otani [5], Mifue Taminato [5], Koichi Tomita [5,6], Tateki Kubo [5], Mari Wataya-Kaneda [1,2], Atsushi Kumanogoh [7], Manabu Fujimoto [1], Rei Watanabe [1,8]

**Author Affiliations:**

[1] Department of Dermatology, Course of Integrated Medicine, Graduate School of Medicine, Osaka University, Osaka, Japan

[2] Department of Neurocutaneous Medicine, Division of Health Sciences, Graduate School of Medicine, Osaka University, Osaka, Japan

[3] Research Department, Maruho Co, Ltd., Kyoto, Japan

[4] Cutaneous Allergy and Host Defense, Immunology Frontier Research Center (iFReC), Osaka University, Osaka, Japan

[5] Department of Plastic Surgery, Course of Organ Regulation Medicine, Graduate School of Medicine, Osaka University, Osaka, Japan

[6] Department of Plastic and Reconstructive Surgery, Kindai University, Osaka, Japan

[7] Department of Respiratory Medicine and Clinical Immunology, Course of Internal Medicine, Graduate School of Medicine, Osaka University, Osaka, Japan

[8] Department of Medicine for Cutaneous Immunological Diseases, Course of Integrated Medicine, Graduate School of Medicine, Osaka University, Osaka, Japan

**Corresponding author**:

Rei Watanabe, MD, PhD.

Department of Medicine for Cutaneous Immunological Diseases, Course of Integrated Medicine, Graduate School of Medicine, Osaka University, Osaka, Japan

2-2 Yamadaoka, Suita, Osaka 565-0871, Japan

Phone number: +81-6-6879-3031

Fax number: +81-6-6879-3038

E-mail address: rwatanabe@derma.med.osaka-u.ac.jp

**Competing interests**

SN and SM are affiliated with Maruho Co. as employees, but have declared no conflicts of interest related to this research. The remaining authors also declare no

conflicts of interest.

**Funding statement:** This study was supported by a Grant-in-Aid for JSPS Fellows 22KJ2071 (to MK), a Grant-in-Aid for Scientific Research (KAKENHI) 16K19705 (to RW), and a collaborative research grant from Maruho Co (Osaka, Japan).

**Abstract**

Psoriasis is a multifactorial disorder mediated by IL-17-producing T cells, involving immune cells and skin-constituting cells. Semaphorin 4A (Sema4A), an immune semaphorin, is known to take part in T helper type 1/17 differentiation and activation. However, Sema4A is also crucial for maintaining peripheral tissue homeostasis and its involvement in skin remains unknown. Here, we revealed that while Sema4A expression was pronounced in psoriatic blood lymphocytes and monocytes, it was downregulated in the keratinocytes of both psoriatic lesions and non-lesions compared to controls. Imiquimod application induced more severe dermatitis in Sema4A knockout (KO) mice compared to wild-type (WT) mice. The naïve skin of Sema4AKO mice showed increased T cell infiltration and IL-17A expression along with thicker epidermis and distinct cytokeratin expression compared to WT mice, which are hallmarks of psoriatic non-lesions. Analysis of bone marrow chimeric mice suggested that Sema4A expression in keratinocytes plays a regulatory role in imiquimod-induced dermatitis. The epidermis of psoriatic non-lesion and Sema4AKO mice demonstrated mTOR complex 1 upregulation, and the application of mTOR inhibitors reversed the skewed expression of cytokeratins in Sema4AKO mice. Conclusively, Sema4A-mediated signaling cascades can be triggers for psoriasis and targets in the treatment

60 and prevention of psoriasis.

## INTRODUCTION

While the infiltration of immune cells into skin plays a critical role in the development of psoriasis, as evidenced by interleukin (IL) -23/IL-17 axis (Fitch, Harper, Skorcheva, Kurtz, & Blauvelt, 2007; Hawkes, Yan, Chan, & Krueger, 2018; Kim & Krueger, 2017), recent studies have revealed that cells constructing skin structure, such as keratinocytes, fibroblasts, and endothelial cells, also play pivotal roles in the development (Heidenreich, Röcken, & Ghoreschi, 2009; Lowes, Russell, Martin, Towne, & Krueger, 2013; Zhang et al., 2023) and maintenance (Arasa et al., 2019; Francis et al., 2024; Li et al., 2023; Ma et al., 2023; Tan et al., 2015; Zhu et al., 2020) of psoriasis. Among these cells, keratinocytes function as a barrier and produce cytokines, chemokines, and antimicrobial peptides against foreign stimuli, resulting in the activation of immune cells (Ni & Lai, 2020; Zhou, Chen, Cui, Shi, & Guo, 2022).

Semaphorins were initially identified as guidance cues in neural development (Kolodkin, Matthes, & Goodman, 1993; Pasterkamp & Kolodkin, 2003) but are now regarded to play crucial roles in other physiological processes including angiogenesis (Iragavarapu-Charyulu, Wojcikiewicz, & Urdaneta, 2020; Serini, Maione, Giraudo, & Bussolino, 2009), tumor microenvironment (Hui, Tam, Jiao, & Ong, 2019; Jiang et al., 2022; Nakayama, Kusumoto, Nakahara, Fujiwara, & Higashiyama, 2018; Rajabinejad

et al., 2020), and immune systems (Garcia, 2019; Kanth, Gairhe, & Torabi-Parizi, 2021; M. Naito & Kumanogoh, 2023). Semaphorin 4A (Sema4A), one of the immune semaphorins, plays both pathogenic and therapeutic roles in autoimmune diseases (Cavalcanti et al., 2020; He et al., 2023), allergic diseases (Maeda et al., 2019), and cancer (Iyer & Chapoval, 2018; Liu et al., 2018; Y. Naito et al., 2023; Pan, Wang, & Ye, 2016). While Sema4A expression on T cells is essential for T helper type 1 differentiation in the murine *Propionibacterium acnes*-induced inflammation model and delayed-type hypersensitivity model (Kumanogoh et al., 2005), Sema4A amplifies only T helper type 17 (Th17)-mediated inflammation in the effector phase of murine experimental autoimmune encephalomyelitis (Koda et al., 2020). Accordingly, in multiple sclerosis, high serum Sema4A levels correlate with the elevated serum IL-17A, earlier disease onset, and increased disease severity (Koda et al., 2020; Nakatsuji et al., 2012). In anti-tumor immunity, research involving human samples and murine models suggests that Sema4A expressed in cancer cells and regulatory T cells promotes tumor progression (Delgoffe et al., 2013; Liu et al., 2018; Pan et al., 2016), while other reports reveal that Sema4A in cancer cells and dendritic cells bolsters anti-tumor immunity by enhancing CD8 T cell activity (Y. Naito et al., 2023; Suga et al., 2021). In addition to these roles in immune reactions, mice with a point mutation in Sema4A develop retinal

degeneration, suggesting that Sema4A is also crucial for peripheral tissue homeostasis (Nojima et al., 2013). These reports suggest that the role of Sema4A can differ based on the disease, phase, and involved cells.

Herein, we investigated the roles of Sema4A in the pathogenesis of psoriasis by analyzing skin and blood specimens from psoriatic subjects and using a murine model.

## RESULTS

### Epidermal Sema4A expression is downregulated in psoriasis

The analysis of previously-published single-cell RNA-sequencing data from control (Ctl) and psoriatic lesional (L) skin specimens (Kim et al., 2023) revealed detectable expression of *SEMA4A* in keratinocytes, dendritic cells, and macrophages in both Ctl and L. *SEMA4A* expression was low in neural crest-like cells, fibroblasts, CD4 T cells, CD8 T cells, NK cells, and plasma cells, making the comparison of expression levels impractical (Figure 1A and B; Figure 1-figure supplement 1A-C). While dendritic cells and macrophages showed comparable *SEMA4A* expression levels between Ctl and L, expression in keratinocytes was significantly downregulated in L (Figure 1C).

Immunohistochemistry of Ctl and psoriasis demonstrated Sema4A expression in keratinocytes (Figure 1D). The staining intensity of Sema4A in epidermis was significantly lower in both non-lesions (NL) and L than in Ctl (Figure 1E). Relative mRNA expression of *SEMA4A* was also decreased in the epidermis of NL and L compared to Ctl, while it remained comparable in the dermis (Figure 1F). In contrast, the proportions of Sema4A-positive cells were significantly higher in blood CD4 and CD8 T cells, and monocytes in psoriasis compared to Ctl (Figure 1G; Figure 1-figure supplement 2). Serum Sema4A levels, measured by enzyme-linked immunosorbent

121 assay (ELISA), were comparable between Ctl and psoriasis (Figure 1H). These findings
122 demonstrate that the expression profile of Sema4A in psoriasis varies across cell types.
123

124 **Psoriasis-like dermatitis is augmented in Sema4AKO mice**

125 When psoriasis-like dermatitis was induced in wild-type (WT) mice and
126 Sema4A knockout (KO) mice by imiquimod application on ears (Figure 2A), ear
127 swelling on day 4 was more pronounced in Sema4AKO mice (Figure 2B) with
128 upregulated *Il17a* gene expression (Figure 2C). Flow cytometry analysis of cells
129 isolated from the ears revealed increased proportions of $V\gamma2^{+}$ T cells, $V\gamma2^{-}V\gamma3^{-}$ double-
130 negative (DN) γδ T cells, and IL-17A-producing cells of those fractions in Sema4AKO
131 epidermis (Figure 2D and E; Figure 2-figure supplement 1). In Sema4AKO dermis,
132 there was also an increase in the proportions of $V\gamma2^{+}$ T cells and IL-17A-producing
133 $V\gamma2^{+}$ T cells (Figure 2D and E). These results suggest that Sema4A deficiency in mice
134 accelerates psoriatic profile. IL-17A-producing T cells in skin-draining lymph nodes
135 (dLN) remained comparable between WT mice and Sema4AKO mice (Figure 2F).
136

137 **Sema4A in keratinocytes may play a role in preventing murine psoriasis-like**
138 **dermatitis**

139 To investigate the cells responsible for the augmented ear swelling in
140 Sema4AKO mice, bone marrow chimeric mice were next analyzed (Figure 3A). Mice
141 deficient in non-hematopoietic Sema4A (WT→KO) displayed more pronounced ear
142 swelling than mice with intact Sema4A expression (WT→WT) following imiquimod
143 application (Figure 3B). Similarly, mice with a systemic deficiency of Sema4A
144 (KO→KO) showed severe ear swelling compared to mice deficient in hematopoietic
145 Sema4A (KO→WT) (Figure 3B). Ear swelling was comparable between WT→WT
146 mice and KO→WT mice (Figure 3B). Flow cytometry analysis revealed increased
147 infiltration of IL-17A-producing DN γδ T cells in the epidermis, as well as $V\gamma2^+$ T cells
148 and IL-17A-producing $V\gamma2^+$ T cells in the dermis, in WT→KO mice compared to
149 WT→WT mice (Figure 3C and D). These findings suggest that non-hematopoietic cells,
150 possibly keratinocytes, are primarily responsible for the increased imiquimod-induced
151 Sema4AKO mice ear swelling.
152

153 **Sema4AKO epidermis is thicker than WT epidermis with increased γδ T17**
154 **infiltration**

155 Even without imiquimod application, Sema4AKO ears turned out to be slightly
156 but significantly thicker than WT ears on week 8 while their appearance remained

157 normal (Figure 4A). While epidermal thickness of back skin was comparable at birth
158 (Figure 4B), on week 8, ear epidermis of Sema4AKO mice was notably thicker than
159 that of WT mice (Figure 4B), suggesting that acanthosis in Sema4AKO mice is
160 accentuated post-birth. Dermal thickness remained comparable between WT mice and
161 Sema4AKO mice at both times (Figure 4B). WT epidermis showed significantly higher
162 *Sema4a* mRNA expression compared to the WT dermis (Figure 4C). Based on these
163 observations, Sema4A appears to play a more pronounced role in epidermis than in
164 dermis.

165 Sema4AKO epidermis exhibited increased expression of *Ccl20, Tnfα*, and
166 *Il17a* and a trend of upregulation of *S100a8* compared to WT epidermis (Figure 4D).
167 These differences were not observed in dermis (Figure 4D). Flow cytometry analysis
168 revealed increased infiltration of γδ T cells in Sema4AKO ear (Figure 4E). These cells
169 predominantly expressed resident memory T cell ($T_{RM}$)-characteristic molecules, CD69
170 and CD103 (Figure 4E). Sema4AKO skin also had a higher number of $T_{RM}$ in both CD4
171 and CD8 T cells (Figure 4E). The percentages of $V\gamma2^+$ T cells, DNγδ T cells, and CD8 T
172 cells in epidermis were higher in Sema4AKO mice than in WT mice, which was not the
173 case in dermis (Figure 4F). The proportion of $V\gamma3^+$ dendritic epidermal T cells was
174 comparable between WT mice and Sema4AKO mice (Figure 4F). Epidermal $V\gamma2^+$ T

175 cells and DNγδ T cells in Sema4AKO mice showed higher IL-17A-producing capability
176 (Figure 4G), while IFNγ and IL-4 production was comparable between WT mice and
177 Sema4AKO mice (Figure 4-figure supplement 1A and B). Conversely, the frequency of
178 IL-17A-producing T cells from dLN was comparable (Figure 4-figure supplement 1C).
179 The production of IL-17A and IFNγ from splenic T cells under T17-polarizing
180 conditions remained consistent between WT mice and Sema4AKO mice (Figure 4-
181 figure supplement 2).

182 Taken together, it is suggested that T17 cells are specifically upregulated in
183 epidermis, indicating that the epidermal microenvironment plays a pivotal role in
184 facilitating the increased T cell infiltration observed in naïve Sema4AKO mice.

185

186 **Sema4AKO skin shares features with human psoriatic NL**

187 Previous literatures have identified certain features common to psoriatic L and
188 NL, such as thickened epidermis (Figure 5-figure supplement 1) (Gallais Sérézal et al.,
189 2019), CCL20 upregulation (Gallais Sérézal et al., 2019), and accumulation of IL-17A-
190 producing T cells (Vo et al., 2019), which were detected in Sema4AKO mice.

191 Gene expression analysis using public RNA-sequencing data (Tsoi et al., 2019)
192 with RaNA-seq (Prieto & Barrios, 2019) showed upregulation of keratinization and

193 antimicrobial peptide genes in NL compared to Ctl (Figure 5A). Gene Ontology analysis
194 highlighted an upregulation in biological processes, predominantly in peptide cross-
195 linking involved in epidermis formation and keratinocyte differentiation, with a
196 secondary increase in the defense response to viruses in NL (Figure 5B). While the
197 expression of *Keratin (KRT) 10* was comparable between NL and Ctl, upregulation in
198 *KRT5*, *KRT14*, and *KRT16* was observed in NL (Figure 5C).

199 In the murine model, relative expression levels of *Krt10*, *Krt14*, *Krt16*, and
200 *filaggrin* were elevated in Sema4AKO epidermis. (Figure 6A). Immunofluorescence
201 analysis showed that Sema4AKO epidermis had a higher density of keratinocytes
202 positive for Krt5, Krt10, Krt14, and Krt16 compared to WT epidermis (Figure 6B). This
203 upregulation was not observed in back skin at birth (Figure 6-figure supplement 1).
204 Comparable transepidermal water loss between WT mice and Sema4AKO mice
205 indicated preserved skin barrier function in Sema4AKO mice (Figure 6C).

206 Based on these results, it is implied that the epidermis of human psoriatic NL
207 and Sema4AKO mice exhibit shared pathways, potentially leading to an acanthotic
208 state. Combined with the observed acanthosis and increased T17 infiltration in
209 Sema4AKO mice, Sema4AKO skin is regarded to demonstrate the features
210 characteristic of human psoriatic NL.

211

212 **mTOR signaling is upregulated in the epidermis of psoriatic NL and Sema4AKO**

213 **mice**

214 Previous reports have shown that mTOR pathway plays a critical role in

215 maintaining epidermal homeostasis, as evidenced by mice with keratinocyte-specific

216 deficiencies in Mtor, Raptor, or Rictor, which exhibit a hypoplastic epidermis with

217 impaired differentiation and barrier formation (Asrani et al., 2017; Ding et al., 2016;

218 Ding et al., 2020). We thus investigated mTOR pathway in both human and murine

219 epidermis.

220 Immunohistochemical analyses highlighted the increase in phospho-S6 (p-S6),

221 indicating the upregulation of mTOR complex (C) 1 signaling, in the epidermal upper

222 layers of both L and NL compared to Ctl (Figure 7A). The activation of mTORC2 in the

223 epidermis, inferred from phospho-Akt (p-Akt), was scarcely detectable in L, NL, and

224 Ctl (Figure 7A). In the epidermis of WT mice and Sema4AKO mice, the upregulation of

225 both mTORC1 and mTORC2 signaling was observed in Sema4AKO epidermis by

226 immunohistochemistry (Figure 7B). Western blot analysis showed upregulated

227 mTORC1 signaling in Sema4AKO epidermis compared to WT epidermis (Figure 7C).

228 The enhancement of mTORC1 and mTORC2 signaling became obvious in the

229 Sema4AKO epidermis after developing psoriatic dermatitis by imiquimod application
230 (Figure 7D).
231
232 **Inhibition of mTOR signaling modulates cytokeratin expression in Sema4AKO mice**
233 To investigate the contribution of mTORC1 and mTORC2 signaling in the
234 development of psoriatic features in the Sema4AKO epidermis, mTORC1 inhibitor
235 rapamycin and mTORC2 inhibitor JR-AB2-011 were intraperitoneally applied to
236 Sema4AKO mice for 14 days. Although epidermal thickness remained unchanged by
237 the inhibitors (Figure 8A and B), relative gene expression of *Krt5* was significantly
238 upregulated and that of *Krt16* was significantly downregulated after rapamycin
239 application (Figure 8C). While the upregulation of *Il17a* in Sema4AKO epidermis was
240 not clearly modified by rapamycin (Figure 8C), immunofluorescence revealed the
241 decrease in the number of CD3 T cells in Sema4AKO epidermis by rapamycin (Figure
242 8D). We additionally conducted topical application of rapamycin gel and vehicle gel on
243 the left and right ears of Sema4AKO mice, respectively. Although there were no
244 detectable changes in epidermal thickness and epidermal T cell counts, the upregulation
245 of *Krt5* and downregulation of *Krt16* was observed again (Figure 8-figure supplement
246 1). Conversely, the application of JR-AB2-011 resulted in decreased expression of *Krt5*,

247 *Krt10*, and *Krt14* with a trend towards increased *Krt16* expression (Figure 8E). JR-
248 AB2-011 did not influence the number of infiltrating T cells in the epidermis (Figure
249 8F). mTORC1 primarily regulates keratinocyte proliferation, whereas mTORC2 mainly
250 involved in the keratinocyte differentiation through Sema4A-related signaling
251 pathways. The observed similarities in *Il17a* expression following treatment with
252 rapamycin and JR-AB2-011 suggest that the production of these cytokines is not
253 significantly dependent on Sema4A-related mTOR signaling.
254

255 **DISCUSSION**

256 Recent studies have highlighted the significance of IL-17A-producing $T_{RM}$ in
257 psoriatic NL (Cheuk et al., 2014; Gallais Sérézal et al., 2018; Vo et al., 2019; Vu,
258 Koguchi-Yoshioka, & Watanabe, 2021). This condition is also characterized by
259 epidermal thickening with elevated CCL20 expression (Gallais Sérézal et al., 2019) and
260 a distinct cytokeratin expression pattern, marked by increased levels of Krt5, Krt14, and
261 Krt16 (Tsoi et al., 2019) (Figure 5C). Here, we identified that murine Sema4A
262 deficiency could induce these features of psoriatic NL.

263 Sema4A expression in epidermis, but not in dermis, was diminished in
264 psoriatic L and NL compared to Ctl. While Sema4A expression on blood immune cells
265 was upregulated in psoriasis, its serum levels were comparable between Ctl and
266 psoriasis. Despite the reported involvement of increased Sema4A expression on immune
267 cells in the pathogenesis of multiple sclerosis (Koda et al., 2020; Nakatsuji et al., 2012),
268 our results suggest that the diminished expression of Sema4A in skin-constructing cells
269 plays a more prominent role in the pathogenesis of psoriasis than its increased
270 expression on immune cells.

271 In our murine model, regardless of imiquimod application, IL-17A-producing
272 T cells were increased in Sema4AKO skin although their frequency was comparable in

273 dLN of WT mice and Sema4AKO mice. Additionally, the potential for *in vitro* T17
274 differentiation did not differ between T cells from WT mice and Sema4AKO mice.
275 These findings suggest that the absence of Sema4A in the skin microenvironment plays
276 a crucial role in the localized upregulation of IL-17A-producing T cells in Sema4AKO
277 mice.

278 It is well-documented that upregulated mTORC1 signaling promotes the
279 pathogenesis of psoriasis (Buerger, 2018; Karagianni, Pavlidis, Malakou, Piperi, &
280 Papadavid, 2022; Ruf, Andreoli, Itin, Pluschke, & Schmid, 2014), and that rapamycin
281 can partially ameliorate the disease activity in psoriatic subjects and murine models
282 (Bürger et al., 2017; Gao & Si, 2018; Reitamo et al., 2001). Our results using
283 Sema4AKO mice revealed that the inhibition of mTORC1 leads to the downregulation
284 of *Krt16* and that of mTORC2 leads to the downregulation of undifferentiated
285 keratinocytes, while the Sema4AKO epidermal thickening and the upregulated IL-17A
286 signaling is not reversed by mTOR blockade. It is plausible that the downregulation of
287 Sema4A can lead to the upregulation of mTORC1 and mTORC2 signaling in
288 keratinocytes, and the augmented signaling leads to the psoriatic profile of proliferation
289 and differentiation, which is a part of the psoriatic NL disposition.

290 This study has limitations. Sema4A expression in skin cells other than

291 keratinocytes was not thoroughly investigated. However, since single-cell RNA-
292 sequencing has shown that Sema4A is predominantly expressed in keratinocytes,
293 dendritic cells, and macrophages, with a notable reduction in keratinocytes in psoriasis,
294 we infer that keratinocytes are the primary cells responsible for the psoriatic features
295 resulting from Sema4A downregulation. We were not able to determine whether
296 Sema4A functions as a ligand or a receptor in epidermis (Ito & Kumanogoh, 2016;
297 Kumanogoh et al., 2002; Lu et al., 2018; Sun et al., 2017) in this study, either. Although
298 both mTORC1 and mTORC2 signals are upregulated in Sema4AKO epidermis, we
299 were not able to confirm mTORC2 signaling from human skin due to technical
300 limitation and sample limitation, while the results from augmented mTORC2 signal in
301 Sema4AKO mice and the normalization of Krt5 and Krt14 by mTORC2 inhibitor imply
302 the involvement of mTORC2 signal in psoriatic epidermis. The role of Sema4A other
303 than mTOR signaling, which may be involved in the regulation of T17 induction in
304 skin, is not discussed, either. These limitations should be overcome in the near future.

305 In summary, epidermal Sema4A downregulation can reflect the psoriatic non-
306 lesional features. Thus, targeting the downregulated Sema4A and upregulated mTOR
307 signaling in psoriatic epidermis can be a promising strategy for psoriasis therapy and
308 modification of psoriatic diathesis in NL for the prevention of disease development.

309

310 **MATERIALS AND METHODS**

311 **Human sample collection**

312 Psoriatic L and NL skin specimens were acquired from 17 psoriasis patients.
313 Ctl specimens were obtained from 19 subjects who underwent tumor resection or
314 reconstructive surgery. For epidermal-dermal separation, specimens were incubated
315 overnight at 4℃ with 2.5 mg/mL dispase (Wako) in IMDM (Wako). Blood samples
316 were collected from 73 psoriasis and 33 Ctl. In addition to ELISA (Nakatsuji et al.,
317 2012), peripheral blood mononuclear cells were isolated using Ficoll-Paque PLUS
318 density gradient media (Cytiva). Patient details are provided in Supplemental Table 1.

319

320 **Mice**

321 C57BL/6J WT mice were procured from CLEA Japan. Semaphorin 4A KO
322 mice with C57BL/6J background were generated as previously described (Kumanogoh
323 et al., 2005). We examined female mice in order to reduce the result variation. Neonatal
324 mice and female mice aged 8 to 12 weeks, maintained under specific pathogen-free
325 conditions, were used.

326 To develop psoriasis-like dermatitis, 10 mg of 5% imiquimod cream
327 (Mochida) was applied to both ears for 4 consecutive days. Ear thickness was measured

328 using a thickness gauge (Peacock).

329 For bone marrow reconstitution, $2 \times 10^5$ bone marrow cells obtained from the
330 indicated strains were intravenously transferred to recipient mice that had received a
331 single 10 Gy irradiation. The reconstituted mice were subjected to the experiments in 8
332 weeks.

333 In the specified experiments, skin specimens were separated into epidermis and
334 dermis by 5 mg/mL dispase (Wako) in IMDM for 30 minutes at 37°C.

335 Transepidermal water loss measurements were performed on the back skin of
336 mice at week 8 using a Tewameter (Courage and Khazaka Electronic GmbH), according
337 to the manufacturer's instructions.

338

339 **Immunofluorescence and immunohistochemistry**

340 Specimens were fixed in 4% paraformaldehyde phosphate buffer solution
341 (Wako), embedded in paraffin, and sliced into 3-μm thickness on glass slides. After
342 deparaffinization and rehydration, antigen retrieval was performed using citrate buffer
343 (pH 6.0, Nacalai tesque) or TE buffer (pH 9.0, Nacalai tesque).

344 For immunohistochemistry, samples were incubated with 3% $H_2O_2$ (Wako) for
345 5 minutes. After blocking (Agilent), the specimens were incubated with the indicated

346 primary antibodies under specified conditions (Supplemental Table 2). The specimens
347 were applied with the EnVision Detection Systems Peroxidase/DAB, Rabbit/Mouse
348 (Agilent) and counterstained with hematoxylin (Wako). For immunofluorescence, the
349 blocked specimens were incubated with the indicated primary antibodies followed by
350 the secondary antibodies (Table E4). Mounting media with DAPI (VectaShield) was
351 used. Slides were observed using a fluorescence microscope (BZ-700, Keyence). The
352 staining intensity was measured using Fiji software (ImageJ, National Institutes of
353 Health) over lengths of 200 μm in human samples and 100 μm in murine samples. This
354 measurement was taken from five areas of each specimen, and the average score is
355 presented. The average thickness of epidermis and dermis from 10 spots is presented.
356 The number of epidermal cells positive for the indicated cytokeratins was counted per
357 100 μm width, with the average number from 5 areas being presented. Additionally, the
358 numbers of CD3-positive cells in murine ears were counted across 10 fields of 400 μm
359 width, with the total sum being presented.
360

361 **Quantitative reverse transcription polymerase chain reaction (qRT-PCR)**

362 Total RNA was extracted from homogenized skin tissue using Direct-zol RNA
363 MiniPrep Kit (ZYMO Research). cDNA was synthesized by High-Capacity RNA-to-

364 cDNATM Kit (Thermo Fisher Scientific). qPCR was performed using TB Green Premix
365 Ex Taq II (Takara-bio) on a ViiA 7 Real-Time PCR System (Thermo Fisher Scientific).
366 The primers are listed in Supplemental Table 3. Relative gene expression levels were
367 normalized to the housekeeping gene GAPDH using the ΔΔCT technique.
368

369 **Flow cytometry analysis**

370 Single-cell suspensions from murine skin-dLN and spleen were prepared by
371 grinding, filtering, and lysing red blood cells (BioLegend). Skin specimens were minced
372 and digested with 3 mg/mL collagenase III (Worthington Biochemical Corporation) in
373 RPMI 1640 medium (Wako) at 37℃ for 10 minutes for epidermis, and 30 minutes for
374 dermis or whole skin. Cells were surface-stained with directly conjugated monoclonal
375 antibodies (Supplemental Table 4). Dead cells were identified using LIVE/DEAD$^{TM}$
376 Fixable Dead Cell Stain Kit (Thermo Fisher Scientific). To evaluate cytokine
377 production, cells were stimulated with PMA (50 ng/mL, Wako) and ionomycin (1000
378 ng/mL, Wako), plus Golgiplug (BD Biosciences) for 4 hours before surface staining.
379 Fixation, permeabilization, and intracellular cytokine staining were performed using BD
380 Cytofix/Cytoperm$^{TM}$ Fixation/Permeabilization Kit (BD Biosciences) according to the
381 manufacturer's protocol. In specified experiments, the numbers of each cell subset per

382 ear were estimated using CountBright Absolute Counting Beads (Thermo Fisher
383 Scientific). Sample analysis was conducted using BD FACSCanto II (BD Biosciences),
384 and data were analyzed with Kaluza software (Beckman Coulter).
385

386 ***In vitro* Th17 differentiation**

387 Murine splenic T cells were isolated using Pan T Cell Isolation Kit II (Miltenyi
388 Biotec). Two hundred thousand T cells per well were cultured in 96-well plates in the
389 presence of T Cell Activation/Expansion Kit (Miltenyi Biotec) for 2 weeks. The
390 medium was supplemented twice per week with the following recombinant cytokines:
391 mouse recombinant IL-6 (20 ng/mL), IL-1β (20 ng/mL), and IL-23 (40 ng/mL) for the
392 IL-23 dependent Th17 cell condition; IL-6 (20 ng/mL) and TGFβ1 (3 ng/mL) for the IL-
393 23 independent Th17 cell condition; or IL-23 (40 ng/mL) for the IL-23 only Th17 cell
394 condition. The cytokines listed were purchased from BioLegend (Supplemental Table
395 5). Afterward, the cultured cells were processed for flow cytometry analysis.
396

397 **Western blotting**

398 Murine epidermis was lysed using RIPA buffer (Wako) containing proteinase-
399 and protease-inhibitor cocktail (Nacalai tesque). Protein lysates were separated by 10%

400 SuperSepTM Ace (Wako), transferred onto polyvinylidene difluoride membranes (0.45
401 μm, Merck) by Trans-Blot Turbo Transfer System (Bio-Rad). The membrane was
402 blocked with 5% bovine serum albumin and subjected to immunoblotting targeting the
403 indicated proteins overnight 4℃, followed by the application of HRP-conjugated
404 secondary antibody for one hour at room temperature (Supplemental Table 2). WB
405 stripping solution (Nacalai tesque) was used to remove the antibodies for further
406 evaluation.
407
408 **Inhibition of mTOR**
409 Rapamycin (4 mg/kg, Sanxin Chempharma), JR-AB2-011 (400 μg/kg,
410 MedChemExpress) and vehicle were applied intraperitoneally to mice once daily for 14
411 consecutive days. Rapamycin and JR-AB2-011 were dissolved in 100% DMSO and
412 diluted with 40% Polyethylene Glycol 300 (Wako), 5% Tween-80 (Sigma-Aldrich) and
413 45% saline in sequence. For topical application, 0.2% rapamycin gel and vehicle gel
414 were prepared by the pharmaceutical department as previously described (Wataya-
415 Kaneda et al., 2017). Rapamycin gel was applied to the left ear, and vehicle gel to the
416 right ear (10mg/ear) of Sema4AKO, once daily for 14 consecutive days.
417

418 **Data processing of single-cell RNA-sequencing and bulk RNA-sequencing**

419 The raw count matrix data from the previously reported single-cell RNA-
420 sequencing data from GSE220116 (Kim et al., 2023) were imported into Scanpy (1.9.6)
421 using Python for further analyses. For each sample, cells and genes meeting the
422 following criteria were excluded: cells expressing over 200 genes (sc.pp.filter_cells),
423 cells with a high proportion of mitochondrial genes (> 5%), and genes expressed in
424 fewer than 3 cells (sc.pp.filter_genes). Counts were normalized using
425 sc.pp.normalize_per_cell, logarithmized (sc.pp.log1p), and scaled (sc.pp.scale). Highly
426 variable genes were selected using sc.pp.filter_genes_dispersion with the options
427 min_mean = 0.0125, max_mean = 2.5, and min_disp = 0.7.

428 Principal Component analysis was conducted with sc.pp.pca, selecting the 1st
429 to 50th Principal Components for embedding and clustering. Neighbors were calculated
430 with batch effect correction by BBKNN (Polański et al., 2020). Embedding was
431 performed by sc.tl.umap, and cells were clustered using sc.tl.leiden. Some cells were
432 further subclassified in a similar manner. Differentially expressed genes were identified
433 on the cellxgene VIP, with significance defined as *padj* < 0.05.

434 Bulk RNA-sequencing data from GSE121212 (Tsoi et al., 2019) were re-
435 analyzed using RaNAseq (Prieto & Barrios, 2019) for differential expression in Ctl

436 versus psoriatic NL. Our analysis included normalization, differential gene expression
437 (defining significance as *padj* < 0.05), and focused on Gene Ontology biological
438 process analysis. The gene expression was calculated with the transcripts per million
439 values.
440
441 **Statistical analysis**
442 GraphPad Prism 10 software (GraphPad Software) was used for all statistical
443 analyses except for RNA-sequencing. Mann-Whitney test was used for two-group
444 comparisons, while Kruskal-Wallis test followed by Dunn's multiple comparisons test
445 was applied for comparison among three or more groups. Statistical significance was
446 defined as $p < 0.05$ (*), $p < 0.01$ (**), and $p < 0.001$ (***). In the analysis of RNA-
447 sequencing data, statistical significance was defined as *padj* < 0.01 (**), and *padj* <
448 0.001 (***).
449
450 **Study approval**
451 All experiments involving human specimens were in accordance with the
452 Declaration of Helsinki and were approved by the Institutional Review Board in Osaka
453 University Hospital (20158-6). Written informed consent was obtained from all

participants. All murine experiments were approved by Osaka University Animal Experiment Committee (J007591-013) and all procedures were conducted in compliance with the Guidelines for Animal Experimentation established by Japanese Association for Laboratory Animal Science.

**Data availability**

The single-cell RNA-sequencing datasets generated by Kim et al. (Kim et al., 2023) and Tsoi et al. (Tsoi et al., 2019) used in this study are available in the NCBI Gene Expression Omnibus under accession codes GSE220116 and GSE121212, respectively. Values for all data points in graphs are reported in the Source data.

**Acknowledgments**

We express our gratitude to all patients for their participation in this study. This study was supported by a Grant-in-Aid for JSPS Fellows 22KJ2071 (to MK), a Grant-in-Aid for Scientific Research (KAKENHI) 16K19705 (to RW), and a collaborative research grant from Maruho Co (Osaka, Japan).

## REFERENCES


Arasa, J., Terencio, M. C., Andrés, R. M., Marín-Castejón, A., Valcuende-Cavero, F., Payá, M., & Montesinos, M. C. (2019). Defective Induction of COX-2 Expression by Psoriatic Fibroblasts Promotes Pro-inflammatory Activation of Macrophages. *Front Immunol, 10*, 536. doi:10.3389/fimmu.2019.00536

Asrani, K., Sood, A., Torres, A., Georgess, D., Phatak, P., Kaur, H., . . . Lotan, T. L. (2017). mTORC1 loss impairs epidermal adhesion via TGF-beta/Rho kinase activation. *J Clin Invest, 127*(11), 4001-4017. doi:10.1172/JCI92893

Bürger, C., Shirsath, N., Lang, V., Diehl, S., Kaufmann, R., Weigert, A., . . . Wolf, P. (2017). Blocking mTOR Signalling with Rapamycin Ameliorates Imiquimod-induced Psoriasis in Mice. *Acta Derm Venereol, 97*(9), 1087-1094. doi:10.2340/00015555-2724

Buerger, C. (2018). Epidermal mTORC1 Signaling Contributes to the Pathogenesis of Psoriasis and Could Serve as a Therapeutic Target. *Front Immunol, 9*, 2786. doi:10.3389/fimmu.2018.02786

Cavalcanti, C. A. J., Germoglio, V., de Azevêdo Silva, J., Glesse, N., Vianna, P., Cechim, G., . . . Sandrin-Garcia, P. (2020). T-cell specific upregulation of Sema4A as risk factor for autoimmunity in systemic lupus erythematosus and rheumatoid arthritis. *Autoimmunity, 53*(2), 65-70. doi:10.1080/08916934.2019.1704273

Cheuk, S., Wikén, M., Blomqvist, L., Nylén, S., Talme, T., Ståhle, M., & Eidsmo, L. (2014). Epidermal Th22 and Tc17 cells form a localized disease memory in clinically healed psoriasis. *J Immunol, 192*(7), 3111-3120. doi:10.4049/jimmunol.1302313

Delgoffe, G. M., Woo, S. R., Turnis, M. E., Gravano, D. M., Guy, C., Overacre, A. E., . . . Vignali, D. A. (2013). Stability and function of regulatory T cells is maintained by a neuropilin-1-semaphorin-4a axis. *Nature, 501*(7466), 252-256. doi:10.1038/nature12428

Ding, X., Bloch, W., Iden, S., Rüegg, M. A., Hall, M. N., Leptin, M., . . . Eming, S. A. (2016). mTORC1 and mTORC2 regulate skin morphogenesis and epidermal barrier formation. *Nat Commun, 7*, 13226. doi:10.1038/ncomms13226

Ding, X., Willenborg, S., Bloch, W., Wickström, S. A., Wagle, P., Brodesser, S., . . . Eming, S. A. (2020). Epidermal mammalian target of rapamycin complex 2 controls lipid synthesis and filaggrin processing in epidermal barrier formation. *J Allergy Clin Immunol, 145*(1), 283-300.e288.

506 doi:10.1016/j.jaci.2019.07.033
507 Fitch, E., Harper, E., Skorcheva, I., Kurtz, S. E., & Blauvelt, A. (2007).
508 Pathophysiology of psoriasis: recent advances on IL-23 and Th17 cytokines.
509 *Curr Rheumatol Rep, 9*(6), 461-467. doi:10.1007/s11926-007-0075-1
510 Francis, L., McCluskey, D., Ganier, C., Jiang, T., Du-Harpur, X., Gabriel, J., . . .
511 Mahil, S. K. (2024). Single-cell analysis of psoriasis resolution
512 demonstrates an inflammatory fibroblast state targeted by IL-23 blockade. *Nat*
513 *Commun, 15*(1), 913. doi:10.1038/s41467-024-44994-w
514 Gallais Sérézal, I., Classon, C., Cheuk, S., Barrientos-Somarribas, M., Wadman, E.,
515 Martini, E., . . . Eidsmo, L. (2018). Resident T Cells in Resolved Psoriasis
516 Steer Tissue Responses that Stratify Clinical Outcome. *J Invest Dermatol,*
517 *138*(8), 1754-1763. doi:10.1016/j.jid.2018.02.030
518 Gallais Sérézal, I., Hoffer, E., Ignatov, B., Martini, E., Zitti, B., Ehrström, M., &
519 Eidsmo, L. (2019). A skewed pool of resident T cells triggers psoriasis-
520 associated tissue responses in never-lesional skin from patients with
521 psoriasis. *J Allergy Clin Immunol, 143*(4), 1444-1454.
522 doi:10.1016/j.jaci.2018.08.048
523 Gao, M., & Si, X. (2018). Rapamycin ameliorates psoriasis by regulating the
524 expression and methylation levels of tropomyosin via ERK1/2 and mTOR pathways
525 in vitro and in vivo. *Exp Dermatol, 27*(10), 1112-1119. doi:10.1111/exd.13745
526 Garcia, S. (2019). Role of Semaphorins in Immunopathologies and Rheumatic Diseases.
527 *Int J Mol Sci, 20*(2). doi:10.3390/ijms20020374
528 Hawkes, J. E., Yan, B. Y., Chan, T. C., & Krueger, J. G. (2018). Discovery of the IL-
529 23/IL-17 Signaling Pathway and the Treatment of Psoriasis. *J Immunol, 201*(6),
530 1605-1613. doi:10.4049/jimmunol.1800013
531 He, R., Tan, X., Xiang, J., Zhu, J., Jiang, Y., Liu, W., . . . Xing, Y. (2023).
532 Semaphorin 4A as a Potential Biomarker for Diagnosis of Systemic Lupus
533 Erythematosus. *Immunol Invest, 52*(1), 104-116.
534 doi:10.1080/08820139.2022.2134024
535 Heidenreich, R., Röcken, M., & Ghoreschi, K. (2009). Angiogenesis drives psoriasis
536 pathogenesis. *Int J Exp Pathol, 90*(3), 232-248. doi:10.1111/j.1365-
537 2613.2009.00669.x
538 Hui, D. H. F., Tam, K. J., Jiao, I. Z. F., & Ong, C. J. (2019). Semaphorin 3C as a
539 Therapeutic Target in Prostate and Other Cancers. *Int J Mol Sci, 20*(3).
540 doi:10.3390/ijms20030774
541 Iragavarapu-Charyulu, V., Wojcikiewicz, E., & Urdaneta, A. (2020). Semaphorins in

Angiogenesis and Autoimmune Diseases: Therapeutic Targets? *Front Immunol, 11*, 346. doi:10.3389/fimmu.2020.00346

Ito, D., & Kumanogoh, A. (2016). The role of Sema4A in angiogenesis, immune responses, carcinogenesis, and retinal systems. *Cell Adh Migr, 10*(6), 692-699. doi:10.1080/19336918.2016.1215785

Iyer, A. S., & Chapoval, S. P. (2018). Neuroimmune Semaphorin 4A in Cancer Angiogenesis and Inflammation: A Promoter or a Suppressor? *Int J Mol Sci, 20*(1). doi:10.3390/ijms20010124

Jiang, J., Zhang, F., Wan, Y., Fang, K., Yan, Z. D., Ren, X. L., & Zhang, R. (2022). Semaphorins as Potential Immune Therapeutic Targets for Cancer. *Front Oncol, 12*, 793805. doi:10.3389/fonc.2022.793805

Kanth, S. M., Gairhe, S., & Torabi-Parizi, P. (2021). The Role of Semaphorins and Their Receptors in Innate Immune Responses and Clinical Diseases of Acute Inflammation. *Front Immunol, 12*, 672441. doi:10.3389/fimmu.2021.672441

Karagianni, F., Pavlidis, A., Malakou, L. S., Piperi, C., & Papadavid, E. (2022). Predominant Role of mTOR Signaling in Skin Diseases with Therapeutic Potential. *Int J Mol Sci, 23*(3). doi:10.3390/ijms23031693

Kim, J., & Krueger, J. G. (2017). Highly Effective New Treatments for Psoriasis Target the IL-23/Type 17 T Cell Autoimmune Axis. *Annu Rev Med, 68*, 255-269. doi:10.1146/annurev-med-042915-103905

Kim, J., Lee, J., Li, X., Lee, H. S., Kim, K., Chaparala, V., . . . Krueger, J. G. (2023). Single-cell transcriptomics suggest distinct upstream drivers of IL-17A/F in hidradenitis versus psoriasis. *J Allergy Clin Immunol, 152*(3), 656-666. doi:10.1016/j.jaci.2023.05.012

Koda, T., Namba, A., Kinoshita, M., Nakatsuji, Y., Sugimoto, T., Sakakibara, K., . . . Okuno, T. (2020). Sema4A is implicated in the acceleration of Th17 cell-mediated neuroinflammation in the effector phase. *J Neuroinflammation, 17*(1), 82. doi:10.1186/s12974-020-01757-w

Kolodkin, A. L., Matthes, D. J., & Goodman, C. S. (1993). The semaphorin genes encode a family of transmembrane and secreted growth cone guidance molecules. *Cell, 75*(7), 1389-1399. doi:10.1016/0092-8674(93)90625-z

Kumanogoh, A., Marukawa, S., Suzuki, K., Takegahara, N., Watanabe, C., Ch'ng, E., . . . Kikutani, H. (2002). Class IV semaphorin Sema4A enhances T-cell activation and interacts with Tim-2. *Nature, 419*(6907), 629-633. doi:10.1038/nature01037

Kumanogoh, A., Shikina, T., Suzuki, K., Uematsu, S., Yukawa, K., Kashiwamura,

578 S., . . . Kikutani, H. (2005). Nonredundant roles of Sema4A in the immune
579 system: defective T cell priming and Th1/Th2 regulation in Sema4A-deficient
580 mice. *Immunity, 22*(3), 305-316. doi:10.1016/j.immuni.2005.01.014
581 Li, Q., Shao, S., Zhu, Z., Chen, J., Hao, J., Bai, Y., . . . Wang, G. (2023). An
582 IGFBP7hi endothelial cell subset drives T cell extravasation in psoriasis via
583 endothelial glycocalyx degradation. *J Clin Invest, 133*(9).
584 doi:10.1172/jci160451
585 Liu, X., Sun, Y., Tian, W., Wang, F., Lv, X., Wang, M., . . . Han, M. (2018). Sema4A
586 Responds to Hypoxia and Is Involved in Breast Cancer Progression. *Biol Pharm*
587 *Bull, 41*(12), 1791-1796. doi:10.1248/bpb.b18-00423
588 Lowes, M. A., Russell, C. B., Martin, D. A., Towne, J. E., & Krueger, J. G. (2013).
589 The IL-23/T17 pathogenic axis in psoriasis is amplified by keratinocyte
590 responses. *Trends Immunol, 34*(4), 174-181. doi:10.1016/j.it.2012.11.005
591 Lu, N., Li, Y., Zhang, Z., Xing, J., Sun, Y., Yao, S., & Chen, L. (2018). Human
592 Semaphorin-4A drives Th2 responses by binding to receptor ILT-4. *Nat Commun,*
593 *9*(1), 742. doi:10.1038/s41467-018-03128-9
594 Ma, F., Plazyo, O., Billi, A. C., Tsoi, L. C., Xing, X., Wasikowski, R., . . .
595 Gudjonsson, J. E. (2023). Single cell and spatial sequencing define processes
596 by which keratinocytes and fibroblasts amplify inflammatory responses in
597 psoriasis. *Nat Commun, 14*(1), 3455. doi:10.1038/s41467-023-39020-4
598 Maeda, Y., Tsuda, T., Takeda, Y., Koyama, S., Hayama, Y., Nojima, S., . . . Kumanogoh,
599 A. (2019). SEMA4A promotes eosinophil survival and contributes to eosinophil-
600 mediated allergic diseases. *Allergol Int, 68*(2), 274-276.
601 doi:10.1016/j.alit.2018.10.001
602 Naito, M., & Kumanogoh, A. (2023). The role of semaphorins in allergic diseases.
603 *Allergol Int*. doi:10.1016/j.alit.2023.08.006
604 Naito, Y., Koyama, S., Masuhiro, K., Hirai, T., Uenami, T., Inoue, T., . . .
605 Kumanogoh, A. (2023). Tumor-derived semaphorin 4A improves PD-1-blocking
606 antibody efficacy by enhancing CD8(+) T cell cytotoxicity and proliferation.
607 *Sci Adv, 9*(20), eade0718. doi:10.1126/sciadv.ade0718
608 Nakatsuji, Y., Okuno, T., Moriya, M., Sugimoto, T., Kinoshita, M., Takamatsu,
609 H., . . . Kumanogoh, A. (2012). Elevation of Sema4A implicates Th cell
610 skewing and the efficacy of IFN-$\beta$ therapy in multiple sclerosis. *J Immunol,*
611 *188*(10), 4858-4865. doi:10.4049/jimmunol.1102023
612 Nakayama, H., Kusumoto, C., Nakahara, M., Fujiwara, A., & Higashiyama, S. (2018).
613 Semaphorin 3F and Netrin-1: The Novel Function as a Regulator of Tumor

614 Microenvironment. *Front Physiol, 9*, 1662. doi:10.3389/fphys.2018.01662
615 Ni, X., & Lai, Y. (2020). Keratinocyte: A trigger or an executor of psoriasis? *J*
616 *Leukoc Biol, 108*(2), 485-491. doi:10.1002/jlb.5mr0120-439r
617 Nojima, S., Toyofuku, T., Kamao, H., Ishigami, C., Kaneko, J., Okuno, T., . . .
618 Kumanogoh, A. (2013). A point mutation in Semaphorin 4A associates with
619 defective endosomal sorting and causes retinal degeneration. *Nat Commun, 4*,
620 1406. doi:10.1038/ncomms2420
621 Pan, J. X., Wang, F., & Ye, L. Y. (2016). Doxorubicin-induced epithelial-mesenchymal
622 transition through SEMA 4A in hepatocellular carcinoma. *Biochem Biophys Res*
623 *Commun, 479*(4), 610-614. doi:10.1016/j.bbrc.2016.09.167
624 Pasterkamp, R. J., & Kolodkin, A. L. (2003). Semaphorin junction: making tracks
625 toward neural connectivity. *Curr Opin Neurobiol, 13*(1), 79-89.
626 doi:10.1016/s0959-4388(03)00003-5
627 Polański, K., Young, M. D., Miao, Z., Meyer, K. B., Teichmann, S. A., & Park, J. E.
628 (2020). BBKNN: fast batch alignment of single cell transcriptomes.
629 *Bioinformatics, 36*(3), 964-965. doi:10.1093/bioinformatics/btz625
630 Prieto, C., & Barrios, D. (2019). RaNA-Seq: Interactive RNA-Seq analysis from FASTQ
631 files to functional analysis. *Bioinformatics*.
632 doi:10.1093/bioinformatics/btz854
633 Rajabinejad, M., Asadi, G., Ranjbar, S., Afshar Hezarkhani, L., Salari, F., Gorgin
634 Karaji, A., & Rezaiemanesh, A. (2020). Semaphorin 4A, 4C, and 4D: Function
635 comparison in the autoimmunity, allergy, and cancer. *Gene, 746*, 144637.
636 doi:10.1016/j.gene.2020.144637
637 Reitamo, S., Spuls, P., Sassolas, B., Lahfa, M., Claudy, A., & Griffiths, C. E.
638 (2001). Efficacy of sirolimus (rapamycin) administered concomitantly with a
639 subtherapeutic dose of cyclosporin in the treatment of severe psoriasis: a
640 randomized controlled trial. *Br J Dermatol, 145*(3), 438-445.
641 doi:10.1046/j.1365-2133.2001.04376.x
642 Ruf, M. T., Andreoli, A., Itin, P., Pluschke, G., & Schmid, P. (2014). Ribosomal
643 protein S6 is hyperactivated and differentially phosphorylated in epidermal
644 lesions of patients with psoriasis and atopic dermatitis. *Br J Dermatol,*
645 *171*(6), 1533-1536. doi:10.1111/bjd.13248
646 Serini, G., Maione, F., Giraudo, E., & Bussolino, F. (2009). Semaphorins and tumor
647 angiogenesis. *Angiogenesis, 12*(2), 187-193. doi:10.1007/s10456-009-9138-4
648 Suga, Y., Nagatomo, I., Kinehara, Y., Koyama, S., Okuzaki, D., Osa, A., . . .
649 Kumanogoh, A. (2021). IL-33 Induces Sema4A Expression in Dendritic Cells and

Exerts Antitumor Immunity. *J Immunol, 207*(5), 1456-1467. doi:10.4049/jimmunol.2100076

Sun, T., Yang, L., Kaur, H., Pestel, J., Looso, M., Nolte, H., . . . Worzfeld, T. (2017). A reverse signaling pathway downstream of Sema4A controls cell migration via Scrib. *J Cell Biol, 216*(1), 199-215. doi:10.1083/jcb.201602002

Tan, Y., Wang, Y., Li, L., Xia, J., Peng, S., & He, Y. (2015). Chemokine-like factor 1-derived C-terminal peptides induce the proliferation of dermal microvascular endothelial cells in psoriasis. *PLoS One, 10*(4), e0125073. doi:10.1371/journal.pone.0125073

Tsoi, L. C., Rodriguez, E., Degenhardt, F., Baurecht, H., Wehkamp, U., Volks, N., . . . Weidinger, S. (2019). Atopic Dermatitis Is an IL-13-Dominant Disease with Greater Molecular Heterogeneity Compared to Psoriasis. *J Invest Dermatol, 139*(7), 1480-1489. doi:10.1016/j.jid.2018.12.018

Vo, S., Watanabe, R., Koguchi-Yoshioka, H., Matsumura, Y., Ishitsuka, Y., Nakamura, Y., . . . Fujimoto, M. (2019). CD8 resident memory T cells with interleukin 17A-producing potential are accumulated in disease-naïve nonlesional sites of psoriasis possibly in correlation with disease duration. *Br J Dermatol, 181*(2), 410-412. doi:10.1111/bjd.17748

Vu, T. T., Koguchi-Yoshioka, H., & Watanabe, R. (2021). Skin-Resident Memory T Cells: Pathogenesis and Implication for the Treatment of Psoriasis. *J Clin Med, 10*(17). doi:10.3390/jcm10173822

Wataya-Kaneda, M., Nakamura, A., Tanaka, M., Hayashi, M., Matsumoto, S., Yamamoto, K., & Katayama, I. (2017). Efficacy and Safety of Topical Sirolimus Therapy for Facial Angiofibromas in the Tuberous Sclerosis Complex : A Randomized Clinical Trial. *JAMA Dermatol, 153*(1), 39-48. doi:10.1001/jamadermatol.2016.3545

Zhang, X., Lei, L., Jiang, L., Fu, C., Huang, J., Hu, Y., . . . Zeng, Q. (2023). Characteristics and pathogenesis of Koebner phenomenon. *Exp Dermatol, 32*(4), 310-323. doi:10.1111/exd.14709

Zhou, X., Chen, Y., Cui, L., Shi, Y., & Guo, C. (2022). Advances in the pathogenesis of psoriasis: from keratinocyte perspective. *Cell Death Dis, 13*(1), 81. doi:10.1038/s41419-022-04523-3

Zhu, Z., Chen, J., Lin, Y., Zhang, C., Li, W., Qiao, H., . . . Wang, G. (2020). Aryl Hydrocarbon Receptor in Cutaneous Vascular Endothelial Cells Restricts Psoriasis Development by Negatively Regulating Neutrophil Recruitment. *J Invest Dermatol, 140*(6), 1233-1243.e1239. doi:10.1016/j.jid.2019.11.022

686

687

688 **Figures**

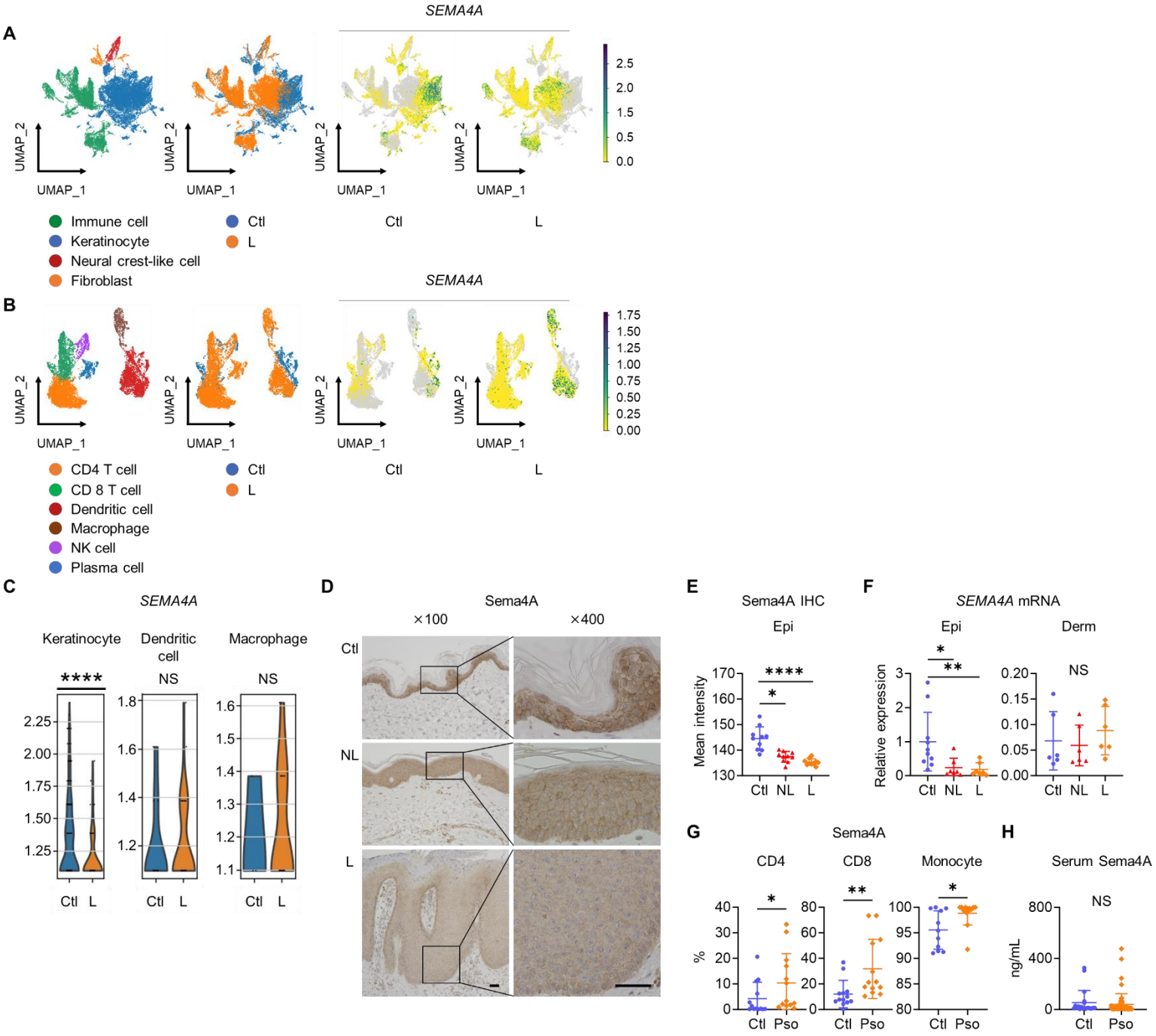


689

690 **Figure 1: Epidermal Sema4A expression is downregulated in psoriasis.**

691 (**A**) UMAP plots, generated from single-cell RNA-sequencing data (GSE220116),

692 illustrate cell distributions from control (Ctl) and psoriatic lesion (L) samples ($n$ = 10
693 for Ctl, $n$ = 11 for L). (**B**) Subclustering of immune cells. (**C**) *SEMA4A* expression in
694 keratinocytes, dendritic cells, and macrophages. ****$padj$ < 0.001. NS, not significant.
695 Analyzed using Python and cellxgene VIP. (**D**) Representative immunohistochemistry
696 and magnified views showing Sema4A expression in Ctl, psoriatic non-lesion (NL), and
697 L. Scale bar = 50 μm. (**E**) Mean epidermal (Epi) Sema4A intensity in
698 immunohistochemistry ($n$ = 10 per group). Each dot represents the average intensity
699 from 5 unit areas per sample. (**F**) Relative *SEMA4A* expression in Epi ($n$ = 10 for Ctl, L,
700 $n$ = 7 for L and NL) and dermis (Derm, $n$ = 6 per group). (**G**) Proportions of Sema4A-
701 expressing cells in blood CD4 T cells (left), CD8 T cells (middle), and monocytes
702 (right) from Ctl and psoriatic (Pso) patients. ($n$ = 13 per group in CD4 and CD8, $n$ = 11
703 for Ctl and $n$ = 13 for Pso in Monocytes). (**H**) Serum Sema4A levels in Ctl ($n$ = 20) and
704 Pso ($n$ = 60). **E** to **H**: *$p$ < 0.05, **$p$ < 0.01, ****$p$ < 0.0001. NS, not significant.
705
706 Figure1-source data1
707 Excel file containing quantitative data for Figure 1.
708

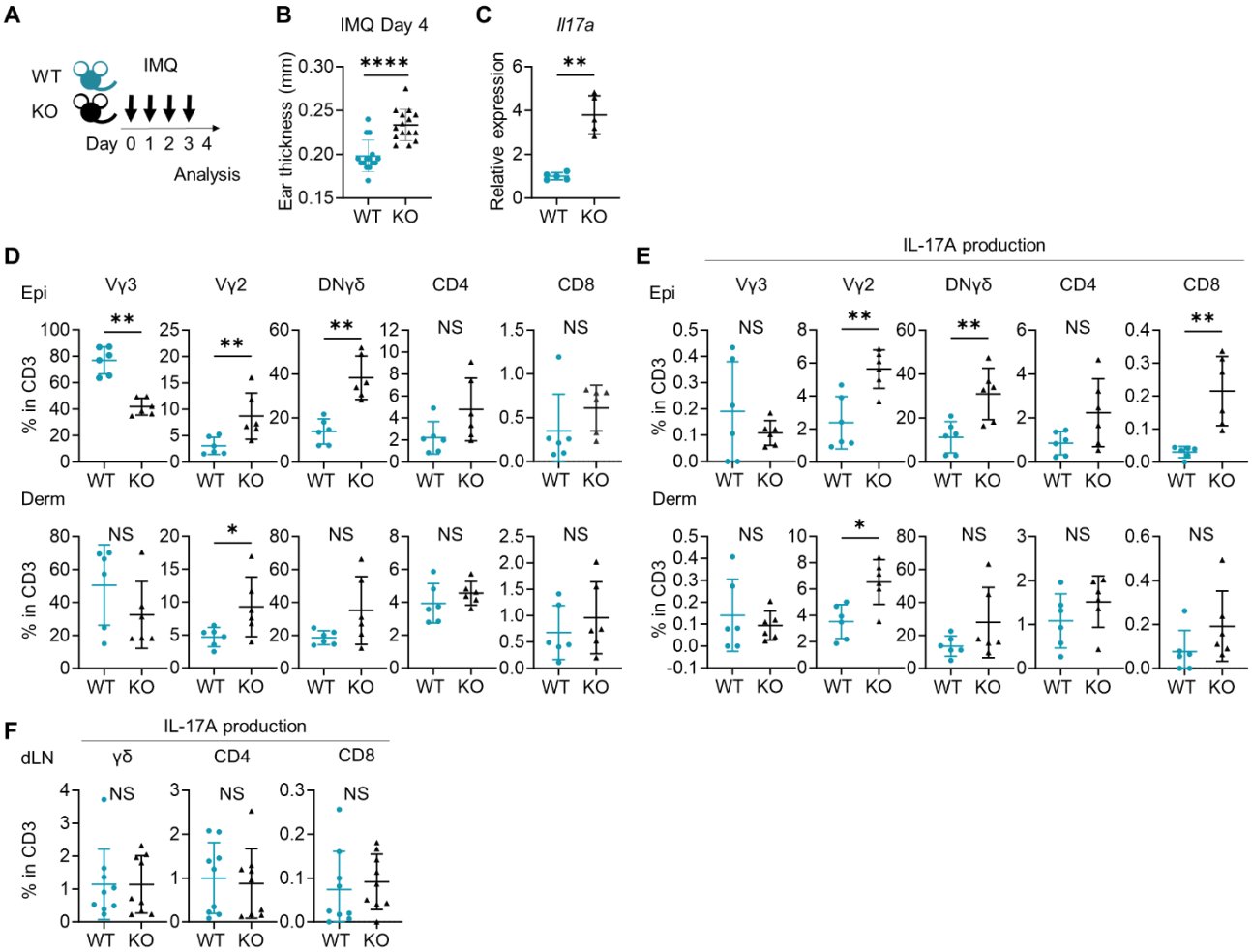


709

710 **Figure 2: Psoriasis-like dermatitis is augmented in Sema4AKO mice.**

711 (**A**) Experimental scheme. Wild-type (WT, green) mice and Sema4A knockout (KO,

712 black) mice were treated with 10 mg/ear of 5% Imiquimod (IMQ) for 4 consecutive

713 days. Samples for flow cytometry analysis were collected on Day 4. (**B**) Ear thickness

714 of WT mice and KO mice on Day 4 ($n$ = 15 per group). (**C**) Relative expression of *Il17a*

715 in epidermis ($n$ = 5 per group). (**D** and **E**) The percentages of Vγ3, Vγ2, Vγ2-Vγ3-γδ

716 (DNγδ), CD4, and CD8 T cells (**D**) and those with IL-17A production (**E**) in CD3

717 fraction in the Epi (top) and Derm (bottom) of WT and KO ears ($n$ = 6 per group, each

718 dot represents the average of 4 ear specimens). (**F**) The percentages of IL-17A-

719 producing γδ, CD4, and CD8 T cells in CD3 fraction in skin-draining lymph nodes

720 (dLN) ($n$ = 9 per group). **B**-**F**: *$p$ < 0.05, **$p$ < 0.01, ****$p$ < 0.0001. NS, not

721 significant.

722

723 Figure2-source data1

724 Excel file containing quantitative data for Figure 2.

725

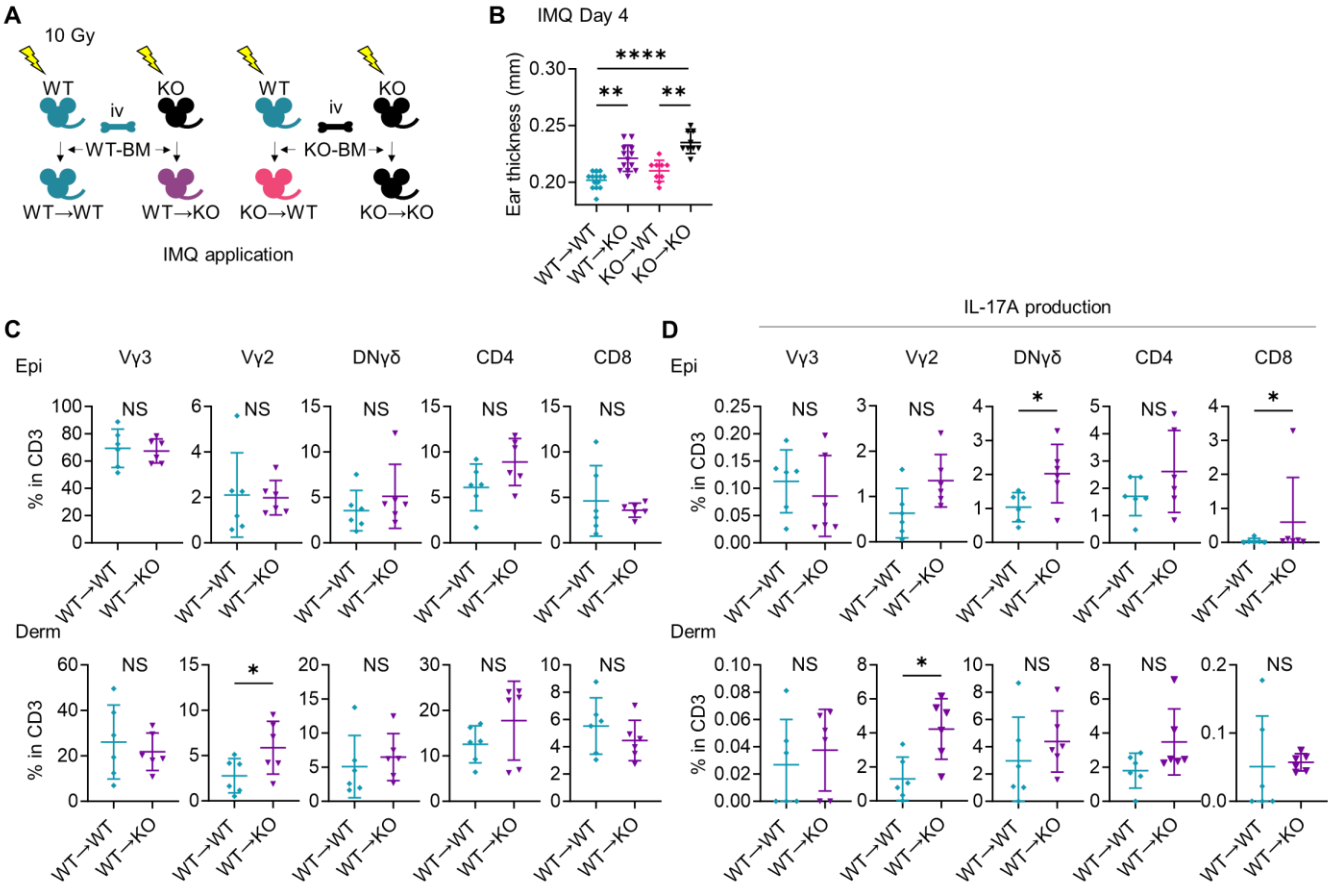


726

727 **Figure 3: Sema4A in keratinocytes may play a role in preventing murine psoriasis-**

728 **like dermatitis.**

729 (**A**) Experimental scheme for establishing BM chimeric mice. (**B**) Day 4 ear thickness

730 in the mice with the indicated genotypes ($n$ = 14 for WT→WT, $n$ = 13 for WT→KO, $n$

731 =9 for KO→WT, $n$ = 9 for KO→KO). (**C** and **D**) The percentages of Vγ3, Vγ2, DNγδ,

732 CD4, and CD8 T cells (**C**) and IL-17A production (**D**) in CD3 fraction from Day 4 Epi

733 (top) and Derm (bottom) of the ears from WT→ WT mice and WT→ KO mice ($n$ = 6

734 per group, each dot represents the average of 4 ear specimens). **B-D**: *$p$ < 0.05, **$p$ <

735 0.01, ****$p < 0.0001$. NS, not significant.

736

737 Figure3-source data1

738 Excel file containing quantitative data for Figure 3.

739

740

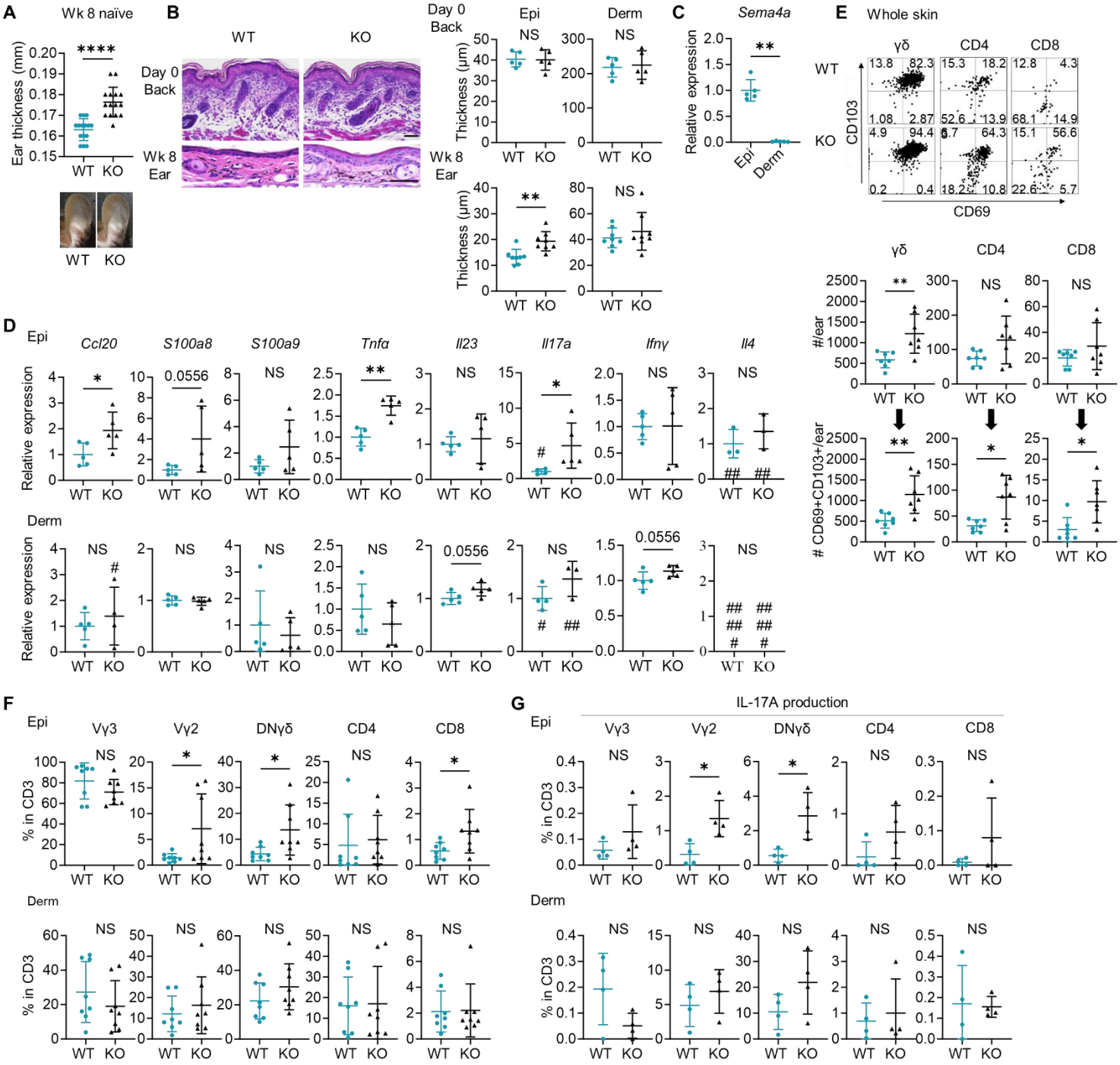


741

742 **Figure 4: Naïve Sema4AKO epidermis is thicker than WT epidermis with**

743 **increased γδ T17 infiltration.**

744 (**A**) Ear thickness of WT mice and KO mice at week (wk) 8 ($n$ = 15 per group) and
745 representative images. (**B**) Left: representative hematoxylin and eosin staining of day 0
746 back and wk 8 ear. Scale bar = 50 μm. Right: Epi and Derm thickness in d 0 back ($n$ =
747 5) and wk 8 ear ($n$ = 8). (**C**) Relative *Sema4a* expression in WT Epi and Derm ($n$ = 5
748 per group). (**D**) Relative expression of psoriasis-associated genes in Epi (top) and Derm
749 (bottom) of WT mice and KO mice ($n$ = 5 per group, #: not detected). (**E**)
750 Representative dot plots showing CD69 and CD103 expression in the indicated T cell
751 fractions from whole skin. The graphs show T cell counts per ear (top) and those with
752 resident memory phenotype (bottom) ($n$ = 7 per group). (**F** and **G**) The percentages of
753 the indicated T cell fractions (**F**, $n$ = 8 per group) and IL-17A production (**G**, $n$ = 4 per
754 group) in Epi (top) and Derm (bottom). **E-G**: Each dot represents the average of 4 ear
755 specimens. **A-G**: *$p < 0.05$, **$p < 0.01$, ****$p < 0.0001$. NS, not significant.
756
757 Figure4-source data1
758 Excel file containing quantitative data for Figure 4.
759

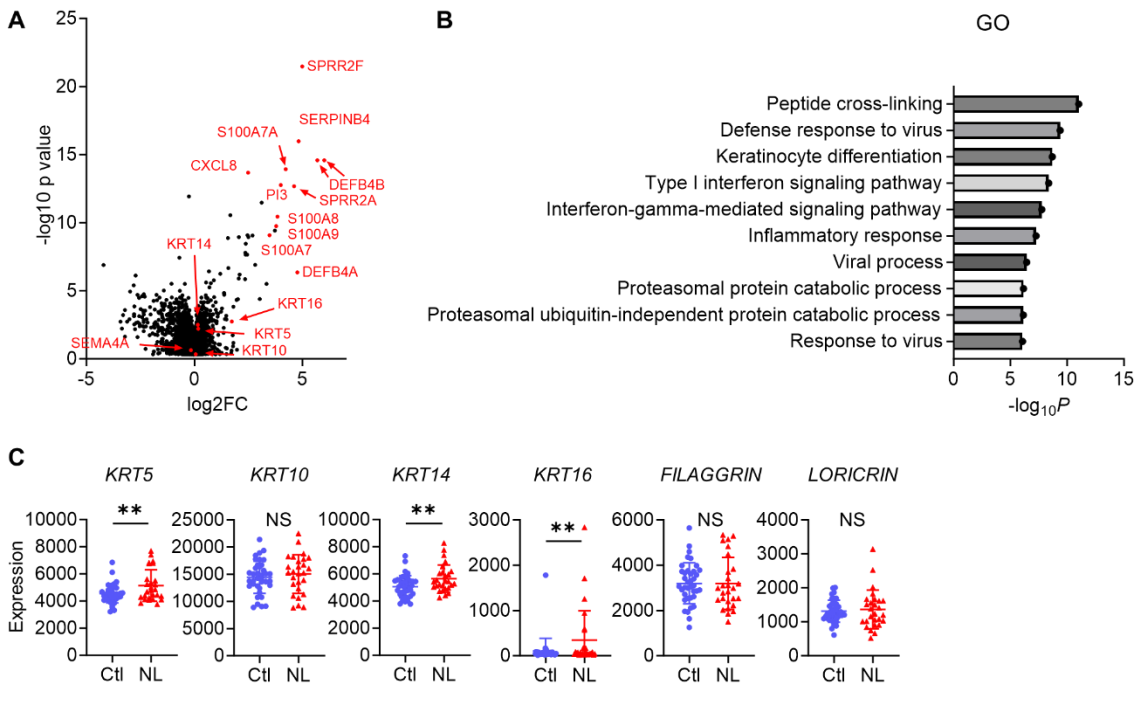


**Figure 5: Psoriatic NL shows aberrant differentiation of keratinocytes**.

(**A** and **B**) The volcano plot (**A**) and Gene ontology (GO) analysis (**B**), generated from RNA-sequencing data (GSE121212) using RaNA-seq, display changes in gene expression in psoriatic NL compared to Ctl. (**C**) The difference in the expression of epidermal differentiation markers between Ctl and NL ($n$ = 38 for Ctl, $n$ = 27 for NL) was calculated with the transcripts per million values. **$padj$ < 0.01. NS, not significant.

Figure5-source data1

Excel file containing quantitative data for Figure 5.

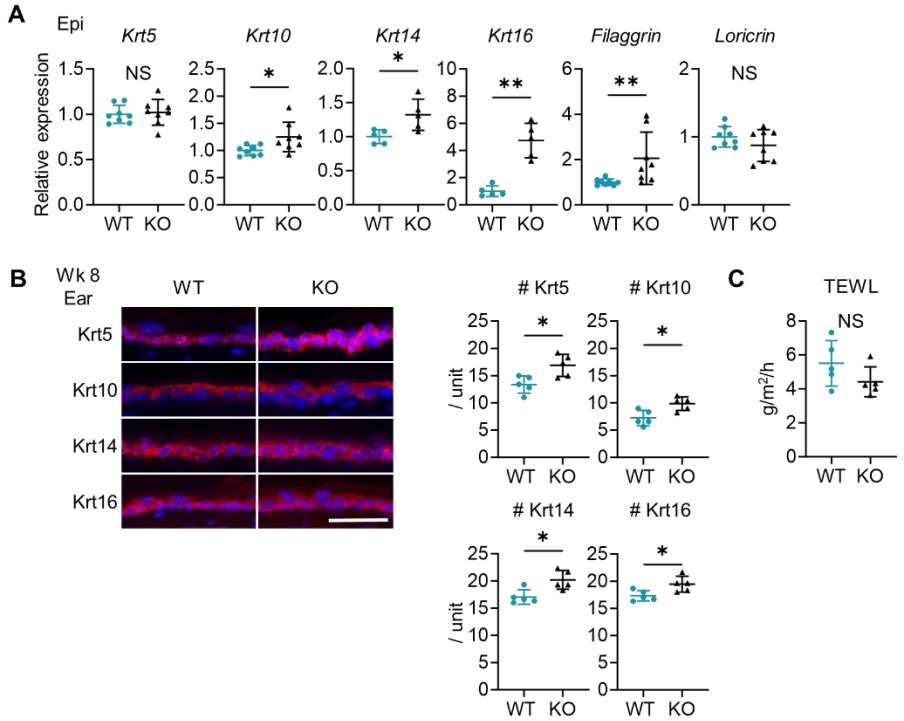


**Figure 6: Sema4AKO skin shares the features of human psoriatic NL.**

(**A**) Relative gene expression of epidermal differentiation markers between wk 8 Epi of WT mice and KO mice ($n$ = 5 for *Krt14* and *Krt16*, $n$ = 8 for *Krt5*, *Krt10*, *Filaggrin,* and *Loricrin*). (**B**) Left: Representative immunofluorescence pictures of Krt5, Krt10, Krt14, and Krt16 (red) overlapped with DAPI. Scale bar = 50 μm. Right: Accumulated graphs showing the numbers of Krt5, Krt10, Krt14, and Krt16 positive cells per 100 μm width ($n$ = 5 per group) of wk 8 ear (right). Each dot represents the average from 5 unit areas per sample. (**C**) Transepidermal water loss (TEWL) in back skin of WT mice and KO mice at wk 8 ($n$ = 5 per group). **A-C**: *$p < 0.05$, **$p < 0.01$. NS, not significant.

Figure 6-source data1

Excel file containing quantitative data for Figure 6.

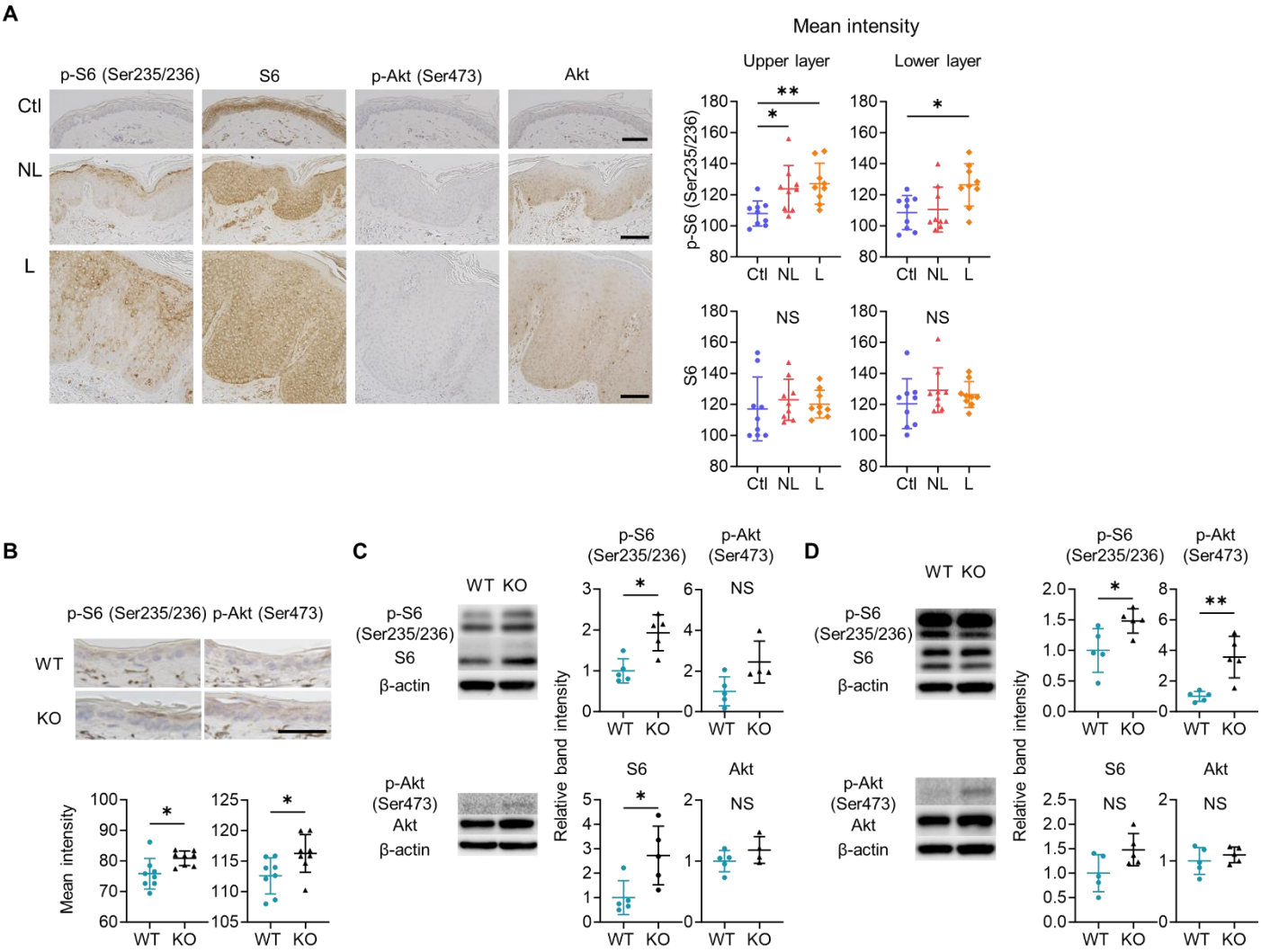


**Figure 7: mTOR signaling is upregulated in the epidermis of psoriatic NL and Sema4AKO mice.**

(**A**) Representative results of immunohistochemistry displaying cells positive for p-S6 (Ser235/236), S6, p-Akt (Ser473), and Akt in Ctl, NL, and L. The graphs of accumulated data show the mean intensity of p-S6 and S6 in the upper and lower epidermal layers ($n$ = 9 per group). Scale bar = 100 μm. Each dot represents the average

795 mean intensity from 5 unit areas per sample. (**B**) The mean intensity of p-S6
796 (Ser235/236) and p-Akt (Ser473), detected by immunohistochemistry in the epidermis
797 of WT mice and KO mice, were analyzed. Scale bar = 50 μm. Each dot represents the
798 average intensity from 5 unit areas per sample ($n$ = 8 per group). (**C** and **D**)
799 Immunoblotting of p-S6 (Ser235/236), S6, p-Akt (Ser473), and Akt in tissue lysates
800 from epidermis without treatment (**C**) and with IMQ treatment for consecutive 4 days
801 (**D**) ($n$ = 5 per group, except for p-Akt and Akt in **C**, for which $n$ = 4). **A**-**D**: *$p < 0.05$,
802 **$p < 0.01$. NS, not significant.
803
804 Figure 7-source data1
805 Excel file containing quantitative data for Figure 7.
806
807

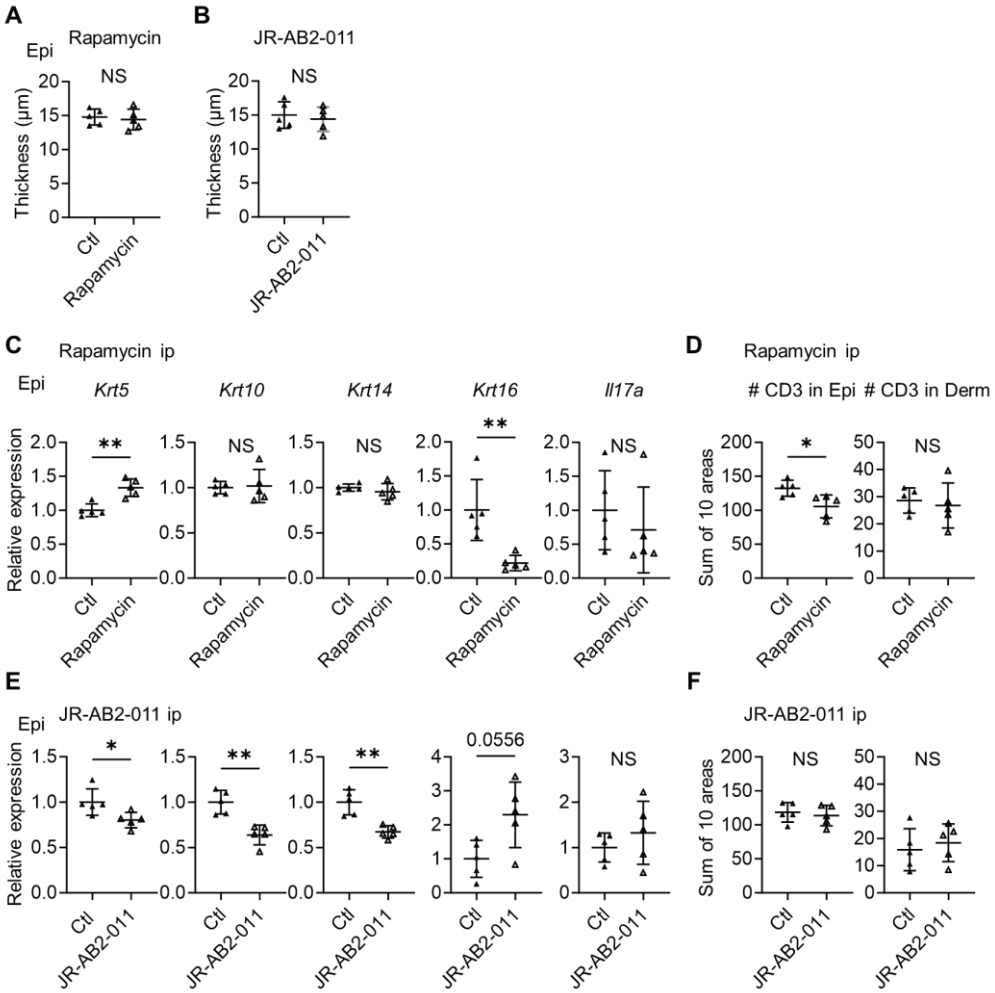


**Figure 8: Inhibitors of mTOR signaling modulate the expression of cytokeratins in Sema4AKO mice.**

(**A** and **B**) Epidermal thickness of Sema4AKO mice treated intraperitoneally with vehicle (Ctl) or rapamycin (**A**), and Ctl or JR-AB2-011 (**B**) ($n$ = 5 per group). (**C** and **D**) Relative expression of keratinocyte differentiation markers and *Il17a* in Sema4AKO Epi (**C**), and the number of T cells in Epi and Derm under Ctl or rapamycin (**D**) ($n$ = 5 per group). (**E** and **F**) Relative expression of keratinocyte differentiation markers and *Il17a* in Sema4AKO Epi (**E**), and the number of T cells in Epi and Derm under Ctl or JR-

817 AB2-011 (**F**) ($n$ = 5 per group). **D** and **F**: Each dot represents the sum of numbers from

818 10 unit areas across 3 specimens. **A**-**F**: *$p < 0.05$, **$p < 0.01$. NS, not significant.

819

820 Figure 8-source data1

821 Excel file containing quantitative data for Figure 8.

822

823

824 **SUPPLEMENTARY MARERIALS**

**A**

| Clinical information | | | | | |
|---|---|---|---|---|---|
| Sample name | Title | Age | Gender | PASI | Site |
| Sample01 | Control01 | 37 | Male | 0 | Trunk |
| Sample02 | Control02 | 37 | Male | 0 | Trunk |
| Sample03 | Control03 | 66 | Male | 0 | Trunk |
| Sample04 | Control04 | 40 | Male | 0 | Leg (right) |
| Sample05 | Control05 | 40 | Male | 0 | Leg (right) |
| Sample06 | Control06 | 41 | Male | 0 | Leg (right) |
| Sample07 | Control07 | 52 | Female | 0 | Arm (left) |
| Sample08 | Control08 | 52 | Female | 0 | Arm (left) |
| Sample09 | Control09 | 74 | Male | 0 | Trunk |
| Sample10 | Control10 | 74 | Male | 0 | Trunk |
| Sample11 | Psoriasis01_preTx_LS | 52 | Female | 18 | Arm (right) |
| Sample12 | Psoriasis02_preTx_LS | 63 | Male | 7.8 | Back |
| Sample13 | Psoriasis03_preTx_LS | 58 | Female | 8.4 | Leg (left) |
| Sample15 | Psoriasis04_preTx_LS | 41 | Male | 9.6 | Trunk |
| Sample17 | Psoriasis05_preTx_LS | 46 | Female | 6.8 | Arm (right) |
| Sample18 | Psoriasis06_preTx_LS | 39 | Male | 6 | Leg (right) |
| Sample21 | Psoriasis07_preTx_LS | 39 | Male | 9.8 | Trunk |
| Sample22 | Psoriasis07_preTx_LS_02 | 40 | Male | 18 | Trunk |
| Sample26 | Psoriasis08_preTx_LS | 48 | Female | 7.4 | Arm (right) |
| Sample27 | Psoriasis09_preTx_LS | 45 | Male | 6.4 | Leg (right) |
| Sample28 | Psoriasis10_preTx_LS | 38 | Male | 8.4 | Leg (right) |

**B**

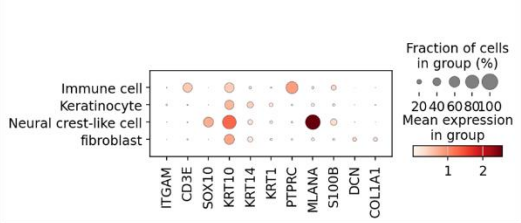


**C**

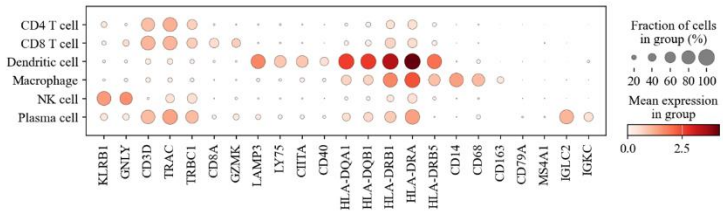


825

826 **Figure 1-figure supplement 1: Sema4A is downregulated in the keratinocytes of**

827 **lesional psoriasis in the single-cell RNA-sequencing data.**

828 (**A**) Sample information for specimens from Ctl and psoriatic L (GSE220116). (**B** and

829 **C**) Clusters of cells were identified by their expression patterns of signature genes.

830

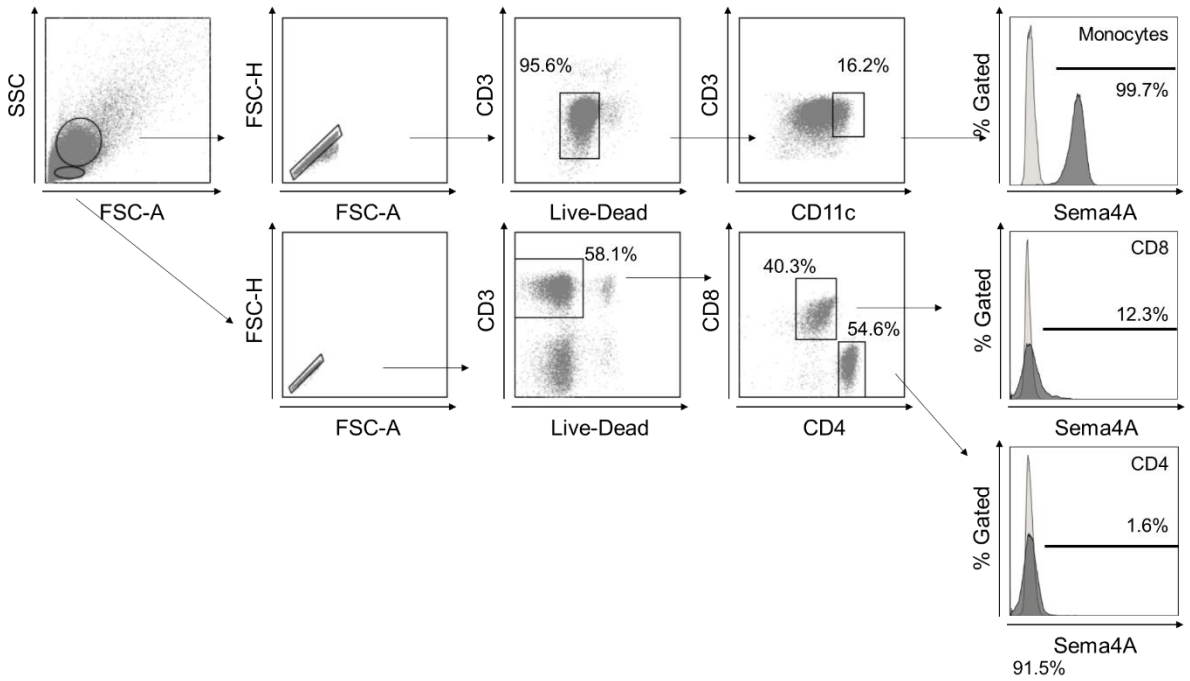


**Figure 1-figure supplement 2: Gating strategy in flow cytometry.**

Gating strategy for human Sema4A expression in blood cells. Large and small cells were distinguished using forward scatter (FCS) and side scatter (SSC) in a dot plot panel, with dead cells being excluded. Monocytes were defined within the live large cell population as CD11c positive. CD4 and CD8 T cells were identified within the live small cell population as CD3 positive CD4 positive and CD3 positive CD8 positive populations, respectively. The empty histogram represents the flow cytometry minus one control for Sema4A.

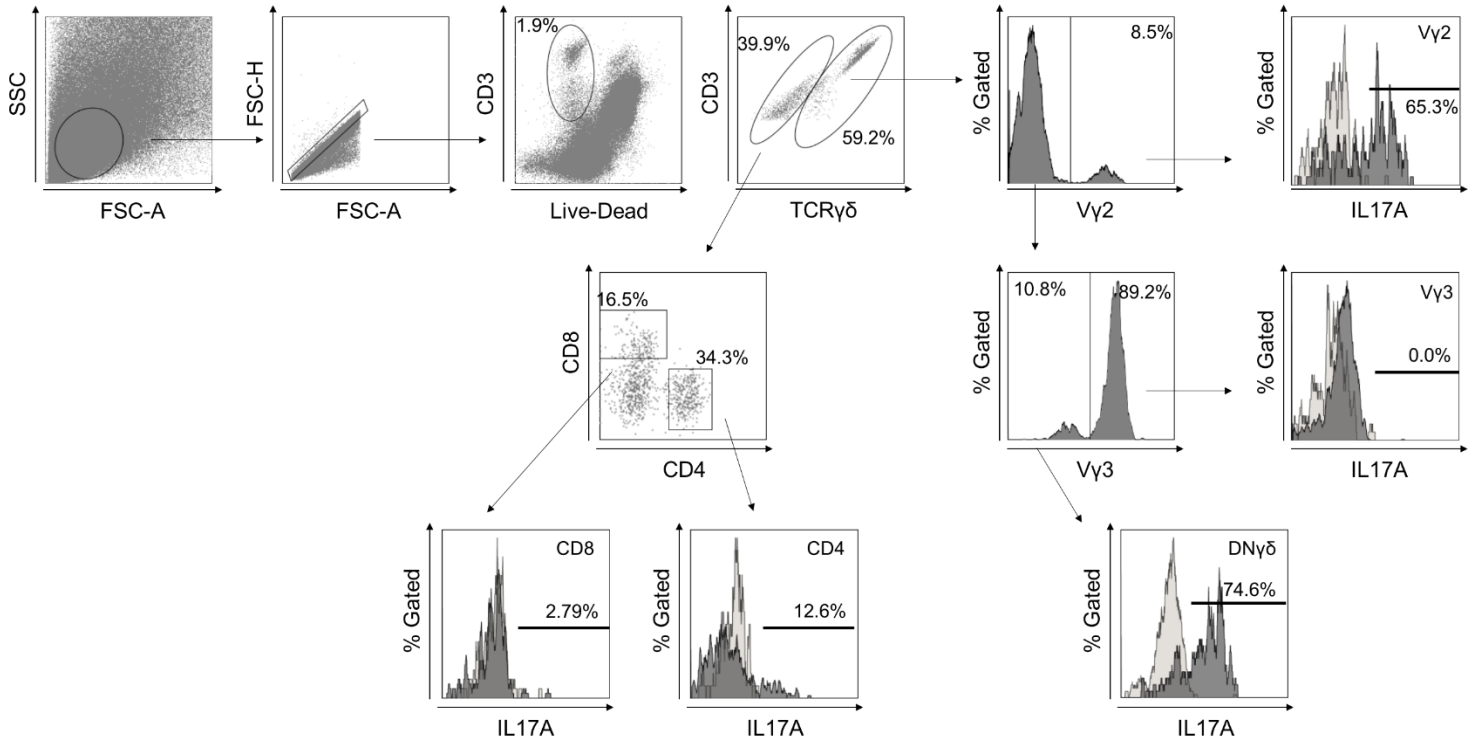


841 **Figure 2-figure supplement 2: Gating strategy in flow cytometry.**

842 Gating strategy for murine T cells infiltrating the epidermis and dermis. After excluding
843 dead cells, TCRγδ positive T cells were evaluated for the expression of Vγ2. TCRγδ
844 positive Vγ2 negative population was further assessed the expression of Vγ3. The CD3
845 positive TCRγδ negative population was evaluated for the expression of CD4 and CD8.
846 Each population was analyzed for cytokine production. The empty histogram represents
847 the isotype control for IL-17A.

848

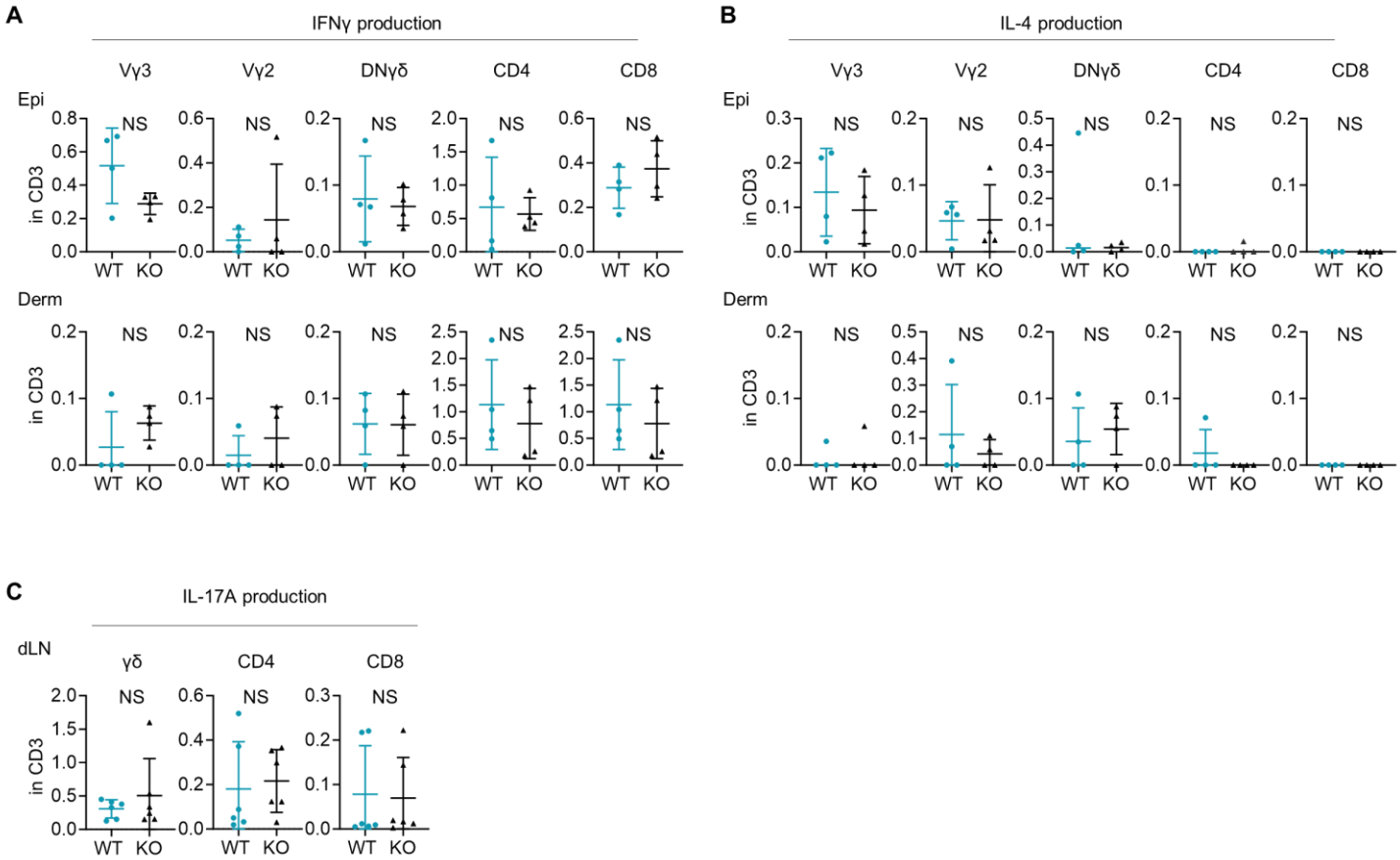


849

850 **Figure 4-figure supplement 1: Expression of IFNγ and IL-4 is comparable between**

851 **WT and Sema4AKO skin.**

852 (**A** and **B**) The graphs presenting the percentages of IFNγ (**A**) and IL-4 (**B**) -producing

853 Vγ2, Vγ2-Vγ3-γδ (DNγδT), CD4, and CD8 T cells in CD3 fraction in the Epi (top) and

854 Derm (bottom) of WT mice and Sema4AKO mice (*n* = 4 per group, each dot represents

855 the average of 4 ear specimens). (**C**) The graphs showing the percentages IL-17A-

856 producing γδ, CD4, and CD8 T cells in CD3 fraction from draining LN (dLN) of WT

857 mice and Sema4AKO mice (*n* = 6 per group). **A-C**: NS, not significant.

Figure 4-figure supplement1-source data1

Excel file containing quantitative data for Figure 4-figure supplement1.

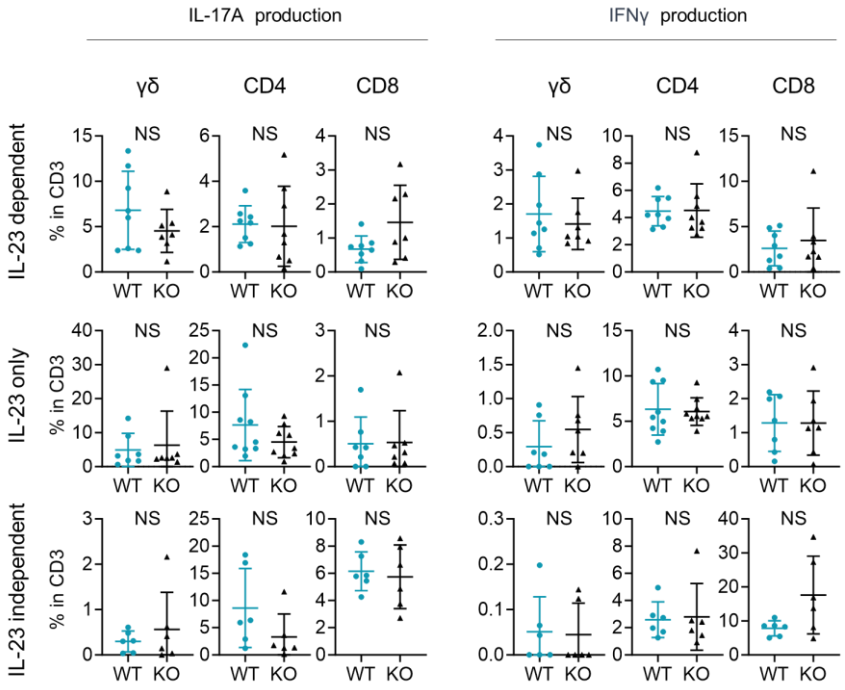


**Figure 4-figure supplement 2: Comparable T17 differentiation potential under Th17-skewing conditions between WT mice and Sema4AKO mice.**

Splenic T cells were cultured for 2 weeks, followed by flow cytometry analysis. The accumulated data display the percentages of IL-17A-producing (right) and IFNγ-producing (left) γδ, CD4, and CD8 T cells within CD3 fraction under various conditions: IL-23 dependent Th17-skewing condition (top), IL-23 only Th17-skewing condition (middle), and IL-23 independent Th17-skewing condition (bottom) . NS, not significant.

Figure 4-figure supplement2-source data1

872 Excel file containing quantitative data for Figure 4-figure supplement2.

873

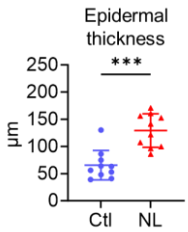


**Figure 5-figure supplement 1: The epidermis of psoriatic non-lesion is thicker than that of control skin.**

Epidermal thickness of Ctl and psoriatic NL ($n$ = 10 per group). ***$p < 0.001$.

Figure 5-figure supplement1-source data1

Excel file containing quantitative data for Figure 5-figure supplement1.

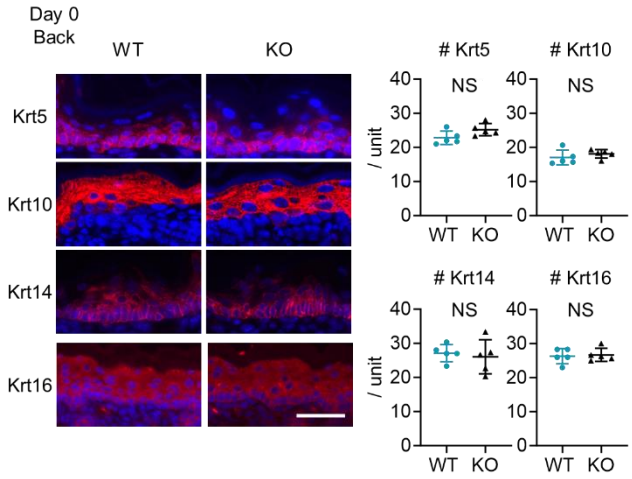


883

884 **Figure 6-figure supplement 1: Upregulation of cytokeratin expression related to**

885 **psoriasis is not detected at birth in Sema4AKO mice.**

886 Representative immunofluorescence pictures of Krt5, Krt10, Krt14, and Krt16 (red)

887 overlapped with DAPI, and the accumulated graphs showing the numbers of Krt5,

888 Krt10, Krt14, and Krt16 positive cells per 100 μm width (*n* = 5 per group) in the

889 epidermis of day 0 back. Scale bar = 50 μm. Each dot represents the average from 5 unit

890 areas per sample. NS, not significant.

891

892 Figure 6-figure supplement1-source data1

893 Excel file containing quantitative data for Figure 6-figure supplement1.

894

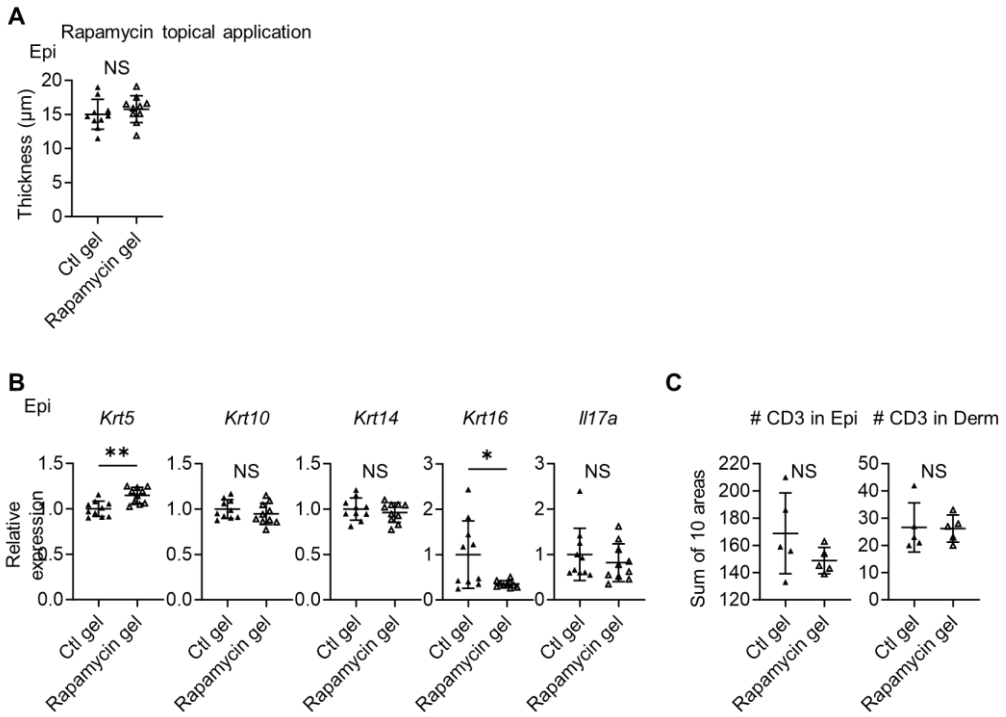


**Figure 8-figure supplement 1: Topical application of rapamycin gel yields partially similar results to intraperitoneal treatment.**

(**A**) Comparison of epidermal thickness between vehicle (Ctl) gel-treated right ears and rapamycin gel-treated left ears of Sema4AKO mice ($n$ = 10 per group). (**B**) Relative expression of keratinocyte differentiation markers and *Il17a* in Sema4AKO Epi under Ctl gel or rapamycin gel treatments ($n$ = 5 per group). (**C**) The number of T cells in the epidermis (left) and dermis (right), under Ctl gel or rapamycin gel treatments ($n$ = 5 per group). Each dot represents the sum of numbers from 10 unit areas across 3 specimens. **A-C**: *$p < 0.05$, **$p < 0.01$. NS, not significant.

906 Figure 8-figure supplement1-source data1

907 Excel file containing quantitative data for Figure 8-figure supplement1.

908

909

Table S1 Patient information

Psoriasis severity is defined by the total body surface area (BSA) affected: <3% BSA for mild, 3%-10% BSA for moderate, and >10% BSA for severe disease.

Fig. 1, D and E Analysis of Sema4A expression by immunohistochemistry

Fig. S4 Epidermal thickness

Psoriasis (n = 10)

| Age | Gender | Body site | Severity |
|---|---|---|---|
| 66 | Male | Leg | Severe |
| 55 | Male | Trunk | Moderate |
| 80 | Female | Trunk | Severe |
| 72 | Male | Trunk | Moderate |
| 30 | Male | Trunk | Severe |
| 72 | Female | Leg | Moderate |
| 63 | Male | Arm | Mild |
| 38 | Male | Trunk | Mild |
| 35 | Male | Leg | Mild |
| 71 | Male | Trunk | Moderate |

Control (n = 10)

| Age | Gender | Body site |
|---|---|---|
| 76 | Male | Neck |
| 52 | Female | Leg |
| 66 | Female | Leg |
| 33 | Male | Leg |
| 68 | Female | Trunk |
| 57 | Female | Leg |
| 65 | Male | Trunk |
| 41 | Female | Trunk |
| 51 | Female | Trunk |
| 66 | Female | Trunk |

Fig 1F Analysis of Sema4A expression by qRT-PCR

Epidermis

Psoriasis (n = 7)

| Age | Gender | Body site | Severity |
|---|---|---|---|
| 71 | Male | Leg | Moderate |
| 76 | Female | Neck | Mild |
| 38 | Female | Trunk | Moderate |
| 49 | Female | Trunk | Moderate |
| 61 | Male | Arm | Mild |
| 68 | Female | Trunk | Moderate |
| 72 | Male | Leg | Mild |

Control (n = 10)

| Age | Gender | Body site |
|---|---|---|
| 57 | Female | Leg |
| 69 | Female | Trunk |

| | | |
|---|---|---|
| 66 | Female | Trunk |
| 86 | Female | Trunk |
| 53 | Female | Trunk |
| 84 | Male | Neck |
| 37 | Female | Trunk |
| 46 | Female | Trunk |
| 51 | Female | Trunk |
| 46 | Female | Trunk |

Dermis

Psoriasis (n = 6)

| Age | Gender | Body site | Severity |
|---|---|---|---|
| 76 | Female | Neck | Mild |
| 38 | Female | Trunk | Moderate |
| 49 | Female | Trunk | Moderate |
| 61 | Male | Arm | Severe |
| 68 | Female | Trunk | Moderate |
| 72 | Male | Leg | Severe |

Control (n = 6)

| Age | Gender | Body site |
|---|---|---|
| 69 | Female | Trunk |
| 86 | Female | Trunk |
| 84 | Male | Neck |
| 37 | Female | Trunk |
| 51 | Female | Trunk |
| 46 | Female | Trunk |

Fig 1G

Analysis of Sema4A expression by flow cytometry

| | Cell type | Average of age | Male (n = ) | Female (n = ) |
|---|---|---|---|---|
| Psoriasis (n = 13) | CD4 T cell, CD8 T cell, and monocyte | 56.1 | 9 | 4 |
| Control (n = 13) | CD4 T cell and CD8 T cell | 52.2 | 6 | 7 |
| Control (n = 11) | Monocyte | 54.1 | 6 | 5 |

Fig 1H

Analysis of Serum Sema4A by ELISA

| | Average of age | Male (n = ) | Female (n = ) |
|---|---|---|---|
| Psoriasis (n = 60) | 55.3 | 43 | 17 |
| Control (n = 20) | 52.1 | 11 | 9 |

Fig 6A

Pictures of p-S6, S6, p-Akt, and Akt staining

Psoriasis (n = 1)

| Age | Gender | Body site | Severity |
|---|---|---|---|
| 30 | Male | Trunk | Severe |

Control (n = 1)

| Age | Gender | Body site |
|---|---|---|
| 66 | Female | Trunk |

Analysis of p-S6, S6 expression by immunohistochemistry

Psoriasis (n = 9)

| Age | Gender | Body site | Severity |
|---|---|---|---|
| 66 | Male | Leg | Severe |
| 55 | Male | Trunk | Moderate |
| 80 | Female | Trunk | Severe |
| 72 | Male | Trunk | Moderate |
| 30 | Male | Trunk | Severe |
| 72 | Female | Leg | Moderate |
| 38 | Male | Trunk | Mild |
| 35 | Male | Leg | Mild |
| 71 | Male | Trunk | Moderate |

Control (n = 9)

| Age | Gender | Body site |
|---|---|---|
| 76 | Male | Neck |
| 66 | Female | Leg |
| 33 | Male | Leg |
| 68 | Female | Trunk |
| 57 | Female | Leg |
| 65 | Male | Trunk |
| 41 | Female | Trunk |
| 51 | Female | Trunk |
| 66 | Female | Trunk |

Table S2
Antibodies used for immunohistochemical, immunofluorescence, and western blot analyses

| Target | Clone | Species | Supplier | Catalog | Dilution | Incubation time | Incubation temperature |
|---|---|---|---|---|---|---|---|
| Sema4A | Polyclonal | Rabbit | Abcom | ab70178 | 100 | 30 min | RT |
| phospho-S6 (Ser235/236) | D57.2.2E | Rabbit | Cell Signaling | 4858 | 400 | overnight | 4 °C |
| S6 | 5G10 | Rabbit | Cell Signaling | 2217 | 100 | overnight | 4 °C |
| phospho-Akt (Ser473) | D9E | Rabbit | Cell Signaling | 4060 | 100 | overnight | 4 °C |
| Akt | C67E7 | Rabbit | Cell Signaling | 4691 | 300 | overnight | 4 °C |
| Keratin 5 | Polyclonal | Rabbit | BioLegend | 905503 | 800 | overnight | 4 °C |
| Keratin 10 | Polyclonal | Rabbit | BioLegend | 905403 | 400 | overnight | 4 °C |
| Keratin 14 | Polyclonal | Rabbit | BioLegend | 905303 | 400 | overnight | 4 °C |
| Cytokeratin 16 | 8L6R4 | Rabbit | Invitrogen | MA5-42892 | 100 | overnight | 4 °C |
| CD3 | CD3-12 | Rat | BIO-RAD | MCA1477 | 100 | overnight | 4 °C |
| Rabbit IgG H&L (Alexa Fluor 555) | Polyclonal | Donkey | Abcam | ab150074 | 1000 | 30 min | RT |
| Rat IgG H&L (Alexa Fluor 555) | Polyclonal | Donkey | Abcam | ab150154 | 1000 | 30 min | RT |
| Rabbit IgG H&L (Alexa Fluor 488) | Polyclonal | Goat | ThermoFisher | A-11034 | 500 | 30 min | RT |
| β-actin | AC-15 | Mouse | Sigma-Aldrich | A5441 | 5000 | overnight | 4 °C |
| Anti-Mouse IgG, HRP-Linked Whole Ab | - | Sheep | Cytiva | NA931 | 10000 | 1 hour | RT |
| Anti-Rabbit IgG, HRP-Linked Whole Ab | - | Donkey | Cytiva | NA934 | 10000 | 1 hour | RT |

RT: Room temperature

Table S3

Primer sequences of real-time quantitative PCR used in human sample experiments

| Gene Symbol | Forward primer (5'-3') | Reverse primer (5'-3') |
|---|---|---|
| *GAPDH* | GTCTCCTCTGACTTCAACAGCG | ACCACCCTGTTGCTGTAGCCAA |
| *SEMA4A* | TCTGCTCCTGAGTGGTGATG | AAACCAGGACACGGATGAAG |

Primer sequences of real-time quantitative PCR in murine sample experiments

| Gene Symbol | Forward primer (5'-3') | Reverse primer (5'-3') |
|---|---|---|
| *Gapdh* | TGTGTCCGTCGTGGATCTGA | TTGCTGTTGAAGTCGCAGGAG |
| *Krt5* | CAGAGCTGAGGAACATGCAG | CATTCTCAGCCGTGGTACG |
| *Krt10* | CGTACTGTTCAGGGTCTGGAG | GCTTCCAGCGATTGTTTCA |
| *Krt14* | CGTACTGTTCAGGGTCTGGAG | GCTTCCAGCGATTGTTTCA |
| *Krt16* | TGAGCTGACCCTGTCCAGA | TGAGCTGACCCTGTCCAGA |
| *Filaggrin* | GGAGGCATGGTGGAACTGA | TGTTTATCTTTTCCCTCACTTCTACATC |
| *Loricrin* | TCACTCATCTTCCCTGGTGCTT | GTCTTTCCACAACCCACAGGA |
| *Sema4a* | ATGGCCCTACCATCCCTGG | AGCAGCGTGTCAAAGTCTCG |
| *Ccl20* | ATGGCCTGCGGTGGCAAGCGT | CATCTTCTTGACTCTTAGGC |
| *S100a8* | TGCGATGGTGATAAAAGTGG | GGCCAGAAGCTCTGCTACTC |
| *S100a9* | CACCCTGAGCAAGAAGGAAT | TGTCATTTATGAGGGCTTCATTT |
| *Ifgγ* | ATCTGGAGGAACTGGCAAAA | TTCAAGACTTCAAAGAGTCTGAGGTA |
| *Tnfα* | GCCTCCCTCTCATCAGTTCT | CACTTGGTGGTTTGCTACGA |
| *Il4* | ACAGGAGAAGGGACGCCAT | GAAGCCCTACAGACGAGCTCA |
| *Il17a* | CTGTGTCTCTGATGCTGTTG | ATGTGGTGGTCCAGCTTTC |
| *Il23* | TCCCTACTAGGACTCAGCCAAC | GCTGCCACTGCTGACTAGAA |

Table S4
Antibodies used for flow cytometry analysis

| Target | Clone | Species | Supplier | Catalog |
|---|---|---|---|---|
| CD3 | OKT3 | Mouse | BioLegend | 317335 |
| CD4 | RPA-T4 | Mouse | BioLegend | 300512 |
| CD8 | RPA-T8 | Mouse | eBioscience | 47-0088-42 |
| CD11c | 3.9 | Mouse | BioLegend | 301628 |
| SEMA4A | 5E3/SEMA4A | Mouse | BioLegend | 148404 |
| CD3ε | 145-2C11 | Armenian Hamster | BioLegend | 100328 |
| CD4 | GK1.5 | Rat | BioLegend | 100406 |
| CD8 | 53-6.7 | Rat | BioLegend | 100714 |
| CD16/32 | 93 | Rat | BioLegend | 101301 |
| CD69 | H1.2F3 | Armenian Hamster | BioLegend | 104514 |
| CD103 | 2E7 | Armenian Hamster | BioLegend | 121422 |
| TCR Vγ2 | UC3-10A6 | Armenian Hamster | BioLegend | 137705 |
| TCR Vγ3 | 536 | Syrian Hamster | BD Biosciences | 743241 |
| TCRγδ | GL3 | Armenian Hamster | BioLegend | 118124 |
| IFNγ | XMG1.2 | Rat | BioLegend | 505813 |
| IL-4 | 11B11 | Rat | BD Biosciences | 562915 |
| IL-17A | TC11-18H10.1 | Rat | BioLegend | 506925 |

Table S5
Mouse recombinant cytokines

| Cytokines | Supplier | Catalog |
|---|---|---|
| IL-1β | BioLegend | 575102 |
| IL-6 | BioLegend | 575702 |
| IL-23 | BioLegend | 589002 |
| TGFβ1 | BioLegend | 763102 |